HHS Public Access

Author manuscript

Cell Host Microbe. Author manuscript; available in PMC 2023 July 28.

Published in final edited form as:

Cell Host Microbe. 2023 February 08; 31(2): 260–272.e7. doi:10.1016/j.chom.2023.01.002.

Structure of the Inmazeb cocktail and resistance to Ebola virus escape

Vamseedhar Rayaprolu[1,6], **Benjamin O. Fulton**[2], **Ashique Rafique**[2], **Emilia Arturo**[1,10], **Dewight Williams**[3], **Chitra Hariharan**[1], **Heather Callaway**[1], **Amar Parvate**[1,7], **Sharon L. Schendel**[1], **Diptiben Parekh**[1], **Sean Hui**[1,8], **Kelly Shaffer**[1,9], **Kristen E. Pascal**[2], **Elzbieta Wloga**[2], **Stephanie Giordano**[2], **Nicole Negron**[2], **Min Ni**[2], **Richard Copin**[2], **Gurinder S. Atwal**[2], **Matthew Franklin**[2], **Ruth Mabel Boytz**[5], **Callie Donahue**[5], **Robert Davey**[5], **Alina Baum**[2], **Christos A. Kyratsous**[2,*], **Erica Ollmann Saphire**[1,4,11,*]

[1]La Jolla Institute for Immunology, La Jolla, CA 92037, USA

[2]Regeneron Pharmaceuticals, Tarrytown, NY 10591, USA

[3]Eyring Materials Center, Arizona State University, Tempe, AZ 85281, USA

[4]Department of Medicine, University of California, San Diego, San Diego, CA 92037, USA

[5]Department of Microbiology, Boston University of Medicine and NEIDL, Boston University, Boston, MA 02118, USA

[6]Present address: Pacific Northwest Center for CryoEM, Portland, OR 97201, USA

[7]Present address: Environmental Molecular Sciences Laboratory, Pacific Northwest National Laboratory, Richland, WA 99354, USA

[8]Present address: Department of Pathology & Immunology, Washington University School of Medicine, St. Louis, MO, USA

[9]Present address: Division of Biology and Biological Engineering, California Institute of Technology, Pasadena, CA 91125, USA

[10]Present address: American Association of Immunologists, Rockville, MD 20852, USA

[11]Lead contact

SUMMARY

[*]Correspondence: christos.kyratsous@regeneron.com (C.A.K.), erica@lji.org (E.O.S.).

AUTHOR CONTRIBUTIONS

Conceptualization, E.O.S., C.A.K., and A.B.; methodology, V.R., B.O.F., A.R., H.C., A.P., K.E.P., R.C., R.D., and E.W.; investigation, V.R., H.C., C.H., B.O.F., A.B., A.R., E.A., K.S., S.H., D.P., E.W., S.G., R.C., K.E.P., R.D., R.M.B., C.D., G.S.A., M.N., and N.N.; formal analysis, V.R., C.H., B.O.F., A.B., A.R., M.F., R.D., and K.E.P.; writing – original draft, V.R., E.O.S., B.O.F., and A.B.; writing – review & editing, V.R., E.O.S., B.O.F., M.F., S.L.S., A.P., C.A.K., and A.B.; visualization, V.R., B.O.F., A.R., and H.C.; supervision, E.O.S., C.A.K., M.F., and A.B.; resources, E.O.S., D.W., C.A.K., A.B., and A.R.; funding acquisition, E.O.S. and C.A.K.

SUPPLEMENTAL INFORMATION

Supplemental information can be found online at https://doi.org/10.1016/j.chom.2023.01.002.

DECLARATION OF INTERESTS

The Regeneron employees have stock and/or options in the company. C.A.K. is an officer of the company. The antibodies are patented: WO/2016/123019.

Monoclonal antibodies can provide important pre- or post-exposure protection against infectious disease for those not yet vaccinated or in individuals that fail to mount a protective immune response after vaccination. Inmazeb (REGN-EB3), a three-antibody cocktail against Ebola virus, lessened disease and improved survival in a controlled trial. Here, we present the cryo-EM structure at 3.1 Å of the Ebola virus glycoprotein, determined without symmetry averaging, in a simultaneous complex with the antibodies in the Inmazeb cocktail. This structure allows the modeling of previously disordered portions of the glycoprotein glycan cap, maps the non-overlapping epitopes of Inmazeb, and illuminates the basis for complementary activities and residues critical for resistance to escape by these and other clinically relevant antibodies. We further provide direct evidence that Inmazeb protects against the rapid emergence of escape mutants, whereas monotherapies even against conserved epitopes do not, supporting the benefit of a cocktail versus a monotherapy approach.

Graphical Abstract

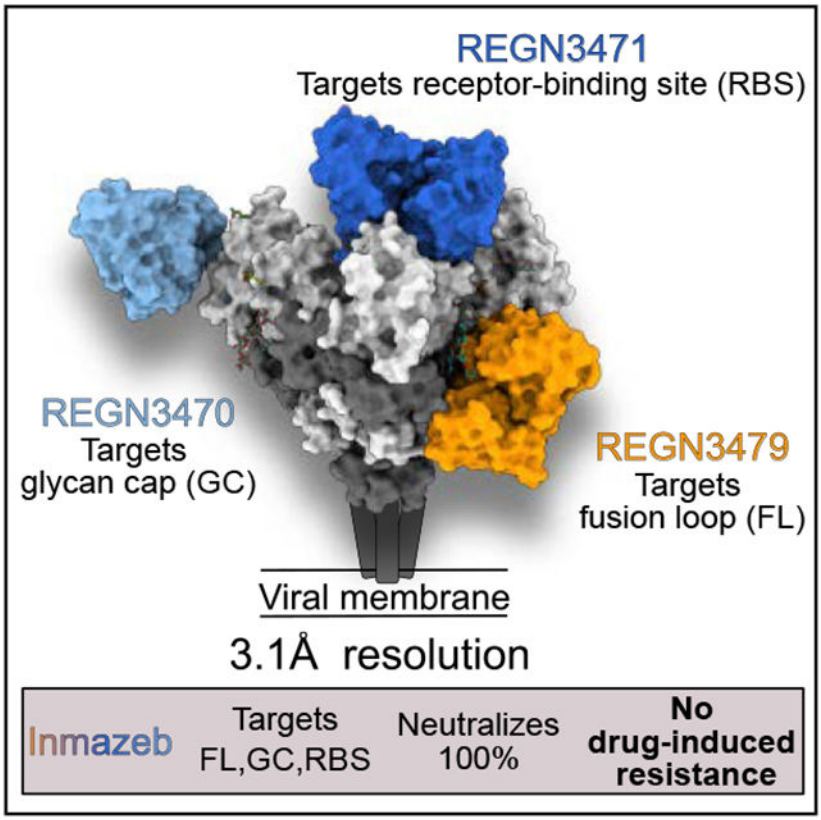

In brief

Rayaprolu et al. combine structural and functional analysis to reveal the molecular details of the Inmazeb antibody cocktail, the first FDA-approved therapeutic effective against Ebola virus disease. They show that targeting non-overlapping epitopes of pathogens is an effective strategy to combat escape mutations and mitigate the risk of drug-induced viral resistance.

INTRODUCTION

Nearly 40 outbreaks of Ebola virus disease (EVD) have occurred, including sustained outbreaks in 2014–2016 of over 28,000 cases and 11,000 deaths, another in 2018 involving 3,300 cases and 2,200 deaths, and a re-emergence in June 2020 that may be linked to recrudescent virus from a survivor of an earlier outbreak.[1] Although an effective vaccine against Ebola virus (EBOV) is available, there are challenges associated with wide-spread vaccination and risk of breakthrough cases in vaccinated individuals.[2] Given the exceptionally high mortality rate, monoclonal antibody (mAb)-based therapeutics remain the most effective treatment for patients infected with EBOV. Although several mAb therapies are in development to treat EBOV infections, REGN-EB3 (Inmazeb) is the first Food and Drug Administration (FDA) approved therapeutic for the treatment of EBOV infection, followed by mAb114 (Ansuvimab) the second.[3]

Therapeutic antibodies against EBOV target the viral glycoprotein (GP). EBOV GP is the only viral protein expressed on the virion surface and is required for host cell attachment, endosomal entry, and membrane fusion. In the producer cell, the GP precursor is cleaved by host furin to yield GP1 and GP2 subunits that remain linked by a disulfide bond.[4] Three GP1-GP2 heterodimers associate and are displayed as trimers on the virus surface.[5] The GP1 subunit drives attachment to target cells and includes the receptor-binding site (RBS), a glycan cap that shields the RBS, and a mucin-like domain (MLD). The GP2 subunit includes a transmembrane (TM) domain that anchors GP in the viral membrane, a stalk, and an internal fusion loop (IFL) that promotes the fusion of the virus with target cell membranes. After macropinocytosis-driven internalization of virions into target cells, endosomal cathepsins process GP and remove the glycan cap and MLD to yield a cleaved version of GP, termed GP_{CL}, which can bind the intra-cellular receptor Niemann-Pick C1 (NPC1).[6] Following receptor binding, GP2 rearranges into a six-helix bundle that drives membrane fusion.[7] In addition to membrane-bound GP, infected cells also produce secreted GP (sGP) that carries the N-terminal 295 amino acids of GP but lacks both the GP2 and MLD.[4] sGP is the primary product of the GP gene and may elicit production of non-neutralizing antibodies that could dampen the effectiveness of the immune response, although its function remains unclear.[8]

Antibodies against GP have been shown to target sites across the entire molecule. Epitopes are found in the membrane-proximal stalk domain, the GP2 fusion loop, the base that includes regions of both GP1 and GP2, and the receptor-binding head, glycan cap, and MLD of GP1. Multiple studies, including a parallel analysis by an international consortium,[9] have determined that a combination of antibody functions correlates with *in vivo* protection, including both neutralization (measured by blocking of infection in cell culture) and induction of multiple immune “effector” functions by the antibody Fc. Some antibodies such as those that bind the GP1 head domain achieve both neutralization and Fc-mediated activities.[9,10] The combination of neutralization and effector functions are also achieved by combining complementary antibodies, for example, in the ZMapp and rE-BOV-520 plus rEBOV-548 cocktails.[11,12]

The REGN-EB3 (Inmazeb) cocktail contains three fully human mAbs[13] that are each directed against a unique, non-overlapping epitope on EBOV GP. The three antibodies in the REGN-EB3 cocktail were selected based on their ability to simultaneously bind EBOV GP and on their complementary combination of functional properties. REGN3479 (maftivimab) targets the fusion loop and is potently neutralizing.[13] REGN3471 (odesivimab) targets the GP1 head and sGP. Although REGN3471 is poorly neutralizing, it mediates effector function and is partially protective in a guinea pig model of EBOV infection. REGN3470 (atoltivimab) targets the glycan cap, is partially neutralizing, and also mediates Fc effector functions that can promote the killing of EBOV-infected cells. During the selection and development of these antibodies, it was hypothesized that a three-antibody cocktail may also reduce the potential for selection of antibody resistance by requiring the simultaneous selection of escape mutations in the GP to each component.[13]

The therapeutic efficacy of the REGN-EB3 cocktail was evaluated in the PALM trial (Pamoja Tulinde Maisha—"Together We Save Lives")—a randomized, controlled trial conducted in the Democratic Republic of the Congo (DRC) during the 2018 EBOV outbreak. This trial compared the efficacy of the triple mAb cocktail ZMapp (control group) with the antiviral agent Remdesivir, the single antibody mAb114, and the REGN-EB3 triple mAb cocktail.[2] The study endpoint was survival at 28 days posttreatment. Patients treated with REGN-EB3 or mAb114 were substantially less likely to die than those treated with ZMapp (percentage surviving: 33.5% and 35.1% death, respectively, vs. 51.3%). In fact, the significantly higher efficacy of REGN-EB3 over ZMapp prompted the early termination of the clinical trial after reviewing 499 of the 700 patients enrolled. These results provided the first clinically evaluated, specific treatment options for EBOV infection. Based on the PALM study results, REGN-EB3 was granted FDA approval as the first antiviral mAb cocktail for the treatment of EVD, the first mAb product for the treatment of a viral infection, and only the second mAb product against a viral antigen.[14]

The lack of high-resolution structure for the REGN-EB3 cocktail in complex with EBOV GP complicates the understanding of the precise contacts that mediate its functions and its complementary activities.[15] Mapping the epitope footprints of these three antibodies can facilitate the monitoring of clinical isolates for GP that carry mutations that are resistant to REGN-EB3. Indeed, the ability of EBOV GP to acquire mutations and develop drug-induced resistance to approved mAb therapeutics has not been previously evaluated. The relevance of *in vitro* viral escape studies with SARS-CoV-2 has now been confirmed in the clinical setting, with the demonstration that monotherapy treatment can select drug-resistant viruses in treated individuals.[16,17]

Here, we report a 3.1 Å resolution cryo-EM structure of the complete REGN-EB3 cocktail simultaneously bound to the EBOV GP trimer. This structure maps the non-overlapping epitopes of REGN-EB3 and illuminates the basis for complementary activities, as well as residues that are critical for resistance to escape by each component of this cocktail and other clinically relevant antibodies. We also provide direct evidence that, unlike monotherapy treatments, including those targeting conserved epitopes, the REGN-EB3 combination protects against the rapid emergence of EBOV escape mutants and supports

the benefit of the combination approach, as has been extensively demonstrated for SARS-CoV-2.[16,18]

RESULTS

To define the structural basis of binding, neutralization, and protection by the REGN-EB3 cocktail of antibodies, we first carried out the cryo-EM analysis of Fabs of the REGN-EB3 cocktail in complex with recombinant, fully glycosylated EBOV GP that lacks the MLD (Mayinga strain, Figure 1A). In initial 2D class averages, complexes were mostly fully occupied with nine Fab fragments (i.e., three copies of each of the three different antibodies). In subsequent 3D classification, the occasional partial occupancy resulted in some classes having nine Fab fragments bound, and others having eight Fab fragments bound (two copies of REGN3470, plus three each of REGN3471 and REGN3479). Homogeneous and non-uniform refinements using Cryo-EM Single Particle Ab-Initio Reconstruction and Classification (cryoSPARC)[19] yielded a cryo-EM reconstruction of the complex resolved to ~3.1 Å. Obtaining a high-resolution map was only possible when particles from both occupancy classes were used for subsequent refinements. Models of the GP and the Fab Fv only were docked into the density and refined (Figures 1B, 1C, S1, and S2; Tables S1 and S2). We determined this structure using C1 symmetry so that individual differences among the monomers can be discerned. All previous cryo-EM structures of EBOV GP at this resolution were determined using C3 symmetry in which the three monomers in the trimer were averaged around the 3-fold axis. There is typically a trade-off between resolution and examination of asymmetry: resolution is improved by averaging monomers together, but biologically relevant individual asymmetric elements are lost during the computational process. For this structure, the application of C3 symmetry and averaging resulted in a loss of signal for all three Fv regions of REGN3470 to the extent that precluded unambiguous model building. By contrast, the C1 symmetry maps revealed clear density for one copy of REGN3470 and moderately strong density for a second copy, which allowed us to build two copies of this antibody into the final structure.

REGN3479 Fab recognizes a quaternary epitope

The REGN3479 Fab binds a quaternary epitope that bridges the paddle-shaped, hydrophobic fusion loop[20] of one GP monomer, monomer A, to a GP1/GP2-containing site in an adjacent monomer, monomer B (Figure 2A). Within this footprint, REGN3479 binds residues 527–530, 535, and 536 of the fusion loop of monomer A, as well as a conformational site involving three polypeptide sections of monomer B and a glycan. This conformational site comprises GP1 residues Pro34, Leu43, and Val45 (β1-β2 strands); GP2 N-terminal residues Ile504, Val 505, and Ala507; GP2 $HR1_A$ residues Gly560, Glu564, and Gln567; and the glycan attached to Asn563 (Figures 2B-2E). In GP2, Leu529 at the tip of the fusion loop was previously shown to bend inward to form a hydrophobic bridge with Ile544. Phe535 interacts with this bridge to form a hydrophobic patch that is required for the formation of a fusion-competent fist-like structure.[21] Phe32 in the REGN3479 light chain (LC) disrupts the formation of this hydrophobic patch formation by wedging between Leu529 and Phe535 of monomer A in the GP trimer (Figure 2C). REGN3479 binding introduces other conformational adjustments on GP as well including a ~180° rotation of Ile527 in the

fusion loop paddle into a hydrophobic pocket created by the heavy-chain (HC) Trp47 and LC Tyr59. Furthermore, residues 549–553 of the fusion loop stem C terminus translate, and residues 552–553 lift to contribute to a helical extension of $HR1_A$ upon REGN3479 binding (Figure 2D).

A primary interaction of REGN3479 Fab is with the conserved GP-linked glycan on Asn563 on monomer B. Tyr49 in REGN3479 LC forms CH-pi stacking interactions with two α-mannose moieties, whereas HC residue Tyr101 stacks with the β-mannose. The side-chain atoms of LC residues Tyr49 and Gln55 and main-chain and side-chain atoms of HC residues Gly100 and Tyr101, respectively, as well as the side-chain atoms of Lys98, Ser104, and Glu106 in the HC sandwich the GP glycan in a network of hydrophobic interactions, hydrogen bonds, and salt bridges (Figure 2B; Table S3).

REGN3471 binds both the head and glycan cap of GP

The epitope footprint of REGN3471 Fab includes both the receptor-binding head (60%) and glycan cap (40%) of GP1 (Figure 1C). GP residues 111–118, which are critical for binding to the cellular NPC1[6] receptor nestle between the HC and LC of REGN3471, and GP residues 143, 144, and 146 interact with all three complementarity determining regions (CDRs) of the HC (Figure 3A). The extended CDR_{L1} of REGN3471 reaches ~10 Å into the RBS to form hydrogen bonds with GP Glu112. Meanwhile, the CDR_{L2} interacts with the glycan linked to Asn238 as well as residues Thr270 and Lys 272 of the glycan cap. This interaction shifts Thr270 by ~9 Å toward the β18 strand (Figures 3B and 3C; Table S3). The partial protection (~33%) achieved in guinea pigs by REGN3471 alone is most likely due to the inhibition of receptor binding, as well as Fc effector functions.

REGN3470 stabilizes the β17/β18 loop in the glycan cap

REGN3470 binds to the top of the glycan cap of GP1 (Figure 1C), at a site involving the antiparallel β17 and β18 strands, which are connected by a 27-residue descending loop (residues 279–306) (Figure 2A). Notably, this structure of the GP-REGN3470 complex allows visualization of the entire β17/18 loop (Figure 4A), which was disordered in all previous structures of EBOV GP. In complex with the REGN3470 Fab, the β17/18 loop of GP is fully ordered, and the main-chain direction as well as the identity and position of the side chains are clear. Interestingly, this clarity occurs only for the two GP monomers that are in complex with the REGN3470 Fab. In the remaining unbound GP monomer, residues 262–270, 280–282, and 293–311 are disordered, similar to previous GP structures.

The β17 and β18 strands of the GP glycan cap are bound by 19 residues of REGN3470, 10 of which interact with Asn278, Glu280, and Asp282 (Table S3). The increased order of the loop connecting the β17 and β18 strands in the REGN-EB3 complex likely arises from the binding of bulky and polar antibody residues in the antibody HC including Asn31, Tyr32, His53, and Asn99. This binding consequentially drives GP residues 277–280 of the β17 strand ~6 Å inward toward the base of GP helix α2. The ordering of the loop creates a new intra-GP backbone interaction between Ile285 and Arg247 that causes the intervening GP residues 281–285 to buckle outward, bringing the entire loop encompassing residues 285–312 into order (Figure 4B). Elsewhere in the glycan cap, LC residues Ser30 and Tyr32

interact with GP residue Ser263 to unravel half a helix turn from the C terminus of α2 and change the position of the loop between the α2 helix and the β17 strand.

Notably, GP residues bound by REGN3470 lie entirely within the glycan cap, which is removed following cleavage in the endosome by cathepsins B and L,[22,23] or other endosomal proteases.[24] Removal of the REGN3470 epitope during viral entry could explain why REGN3470 is a less potent neutralizer but does elicit immune effector functions[13] that require binding to intact GP displayed on cell surfaces.

Glycan cap removal abolishes REGN3470 GP binding and reduces REGN3471 GP binding

Following macropinocytosis, EBOV GP is cleaved by cathepsins in the endosome. This cleavage event removes epitopes contained in the glycan cap and the MLD to produce cleaved GP (GP_{CL}) in which the RBS is exposed to allow binding to the NPC1 receptor.[6] Given that the REGN3470 and REGN3471 at least partially bind the glycan cap, we assessed the ability of all three components of REGN-EB3 and mAb114 to bind both full-length EBOV GP and cleaved EBOV GPcl. To mimic cathepsin B cleavage *in vitro*, we treated GP with thermolysin (ThL) at a molar ratio of 60:1 GP:ThL[25] and then used surface plasmon resonance (SPR) to assess the binding affinity and kinetics of the three antibodies of REGN-EB3 immobilized on the chip surface for GP and GP_{CL}. REGN3479 had a high affinity for GP as evidenced by a K_D of 1.64 nM increased by over 10-fold for GP_{CL} (0.14 nM). Similarly, mAb114 tightly bound both GP and GP_{CL} (0.31 vs. 0.21 nM). REGN3471 had a 4-fold reduction in affinity for GP_{CL} relative to GP (4.4 vs. 15.8 nM). In addition to the reduced affinity, the binding half-life for REGN3471 was reduced by 4-fold. REGN3470 showed no binding to the GP_{CL}, as expected (Figures 5A and S3). The lack of dependence on the glycan cap for REGN3479 and mAb114 binding may allow for enhanced neutralization potency compared with REGN3470 and REGN3471.

We also treated pre-formed individual GP-Fab complexes with ThL and monitored the cleavage event over time using western blotting under non-reducing conditions. Digestion of unbound GP with ThL over time resulted in the disappearance of the major intact GP band (~67 kDa) and the appearance of the major digestion product, GP_{CL} (~37 kDa), as well as an intermediate (~50 kDa) band. Interestingly, ThL digestion of REGN3479 complexed with GP showed a clear reduction in GP_{CL} band intensity and a small increase in the intensity of the larger intermediate (~50 kDa). The marked reduction in GP_{CL} band intensity suggests that the presence of REGN3479 may block the ThL cleavage site (Figure 5B). No discernible difference in cleavage patterns was seen for GP complexed with either REGN3470 or REGN3471 compared with unbound GP (data not shown).

We further evaluated the formation of a stable GP_{CL}-antibody complex using size-exclusion chromatography (SEC). GP_{CL} was incubated with each of the Fabs in the REGN-EB3 cocktail individually, and the elution profile of the complex was monitored using SEC (Figure S4A). GP cleavage did not affect complex formation with REGN3479 as evidenced by the presence of two peaks in the SEC trace, one corresponding to the complex and the other to free Fab. REGN3470 for which the epitope lies exclusively in the glycan cap does not bind cap-deleted GP. Only peaks corresponding to only GP_{CL} and free Fab were observed—with no peak for the complex. REGN3471 for which the glycan cap comprises

~40% of the epitope exhibited some binding of GP_{CL}—three peaks, corresponding to complex, GP_{CL}, and free Fab are observed (Figure S4A).

REGN-EB3 prevents rapid viral escape

We used a chimeric Vesicular stomatitis virus (VSV) expressing EBOV GP (VSV-EBOV-GP) to characterize the likelihood of escape mutations in GP following exposure to individual mAbs and to competing and non-competing antibody combinations. As a first step, we tested the neutralization potency of these antibodies against VSV-EBOV-GP (Figures 6A and 6B). Consistent with previous reports, REGN3479 and mAb114 were potently neutralizing in our assay, with IC50s of 25.9 and 54.7 ng/mL, respectively.[26] REGN3470 also demonstrated high neutralization potency, although neutralization never reached 100%, leaving a small population of infectious virus un-neutralized even at high antibody concentrations (Figure 6C), as previously observed.[13] REGN3471 was poorly neutralizing. The non-competing REGN-EB3 and REGN3479 + mAb114 combinations also potently neutralized VSV-EBOV-GP.

To determine the likelihood of mAb-induced viral escape and identify the mutations in GP associated with loss of therapeutic neutralizing activity, escape studies with VSV-EBOV-G were conducted by passaging the virus in the presence of either individual mAbs or mAbs in combination. Notably, virus resistance characterized by cytopathic cell death was observed within one or two passages for all mAbs used as a monotherapy (Figure 6D). Sequencing analysis revealed that single mutations in the GP protein arising in these one or two passages could result in complete viral resistance to all individual neutralizing mAbs (Figure 6E). Notably, mutations were selected within or adjacent to the contact residues of REGN3470, REGN3471, and REGN3479 (Figure 6E). Mutations that were previously shown to impact antibody neutralization were also selected for other antibodies against EBOV GP including KZ52 (G557R), 2G4 (Q508R), and 4G7 (G557R) mAbs.[27-32]

To understand how epitope conservation correlates with the development of antibody-induced resistance, we assessed the escape kinetics of mAb114 and REGN3479. mAb114 binds to a highly conserved region in the receptor-binding domain (RBD) required for viral entry,[26] while REGN3479 binds the conserved fusion loop and can neutralize multiple ebolaviruses, including EBOV Mayinga, EBOV Mali, Bundibugyo virus, and Sudan virus (Figure S4B). Both mAb114 and REGN3479 rapidly selected resistant viruses within a single passage, similar to all other individual antibodies (Figures 6D and 6E). Furthermore, viruses resistant to mAb114 could be plaque purified and expanded without reversion of the escape mutations or obvious fitness defects.

Next, we assessed the evolution of resistance to antibody cocktails containing components targeting overlapping (ZMapp) or distinct epitopes (REGN-EB3 and REGN3479 + mAb114). Similar to the monotherapies, the selection of a single variant (Q508R) led to complete escape from the triple ZMapp combination containing two neutralizing antibodies that bind overlapping epitopes (2G4 and 4G7; both of which are affected by Q508R) plus one non-neutralizing antibody (13C6). Q508R was also identified in an EBOV-infected cynomolgus macaque that succumbed to the virus after ZMapp therapy and led to resistance to the cocktail, confirming that similar mutations are selected *in vitro* with the pseudotyped

virus *in vivo* with authentic EBOV.[28] However, combinations of three (REGN-EB3) or two (REGN3479 + mAb114) antibodies directed against distinct epitopes increased resistance to viral escape. Ten passages and multiple mutations were required to escape the potently neutralizing two-mAb combination (REGN3479 + mAb114). The emergence of complete resistance was not observed with REGN-EB3 following 10 passages (Figure 6E).

To validate the mutants detected through sequencing analysis, we generated lentivirus-based pseudoparticles (EBOVpp) bearing individual escape mutations within the 2014 Zaire EBOV GP sequence. As expected, the neutralization potency of every individual neutralizing mAb was impacted by mutations detected during selection (Table 1; Figure S5). Two identified mutants (P34S and T469I) did not impact antibody potency. These were likely tissue culture adaptations or were genetically linked to other variants that affect antibody neutralization selected during passaging. Despite the conservation of the mAb114 epitope, four mutants isolated under either mAb114 monotherapy or REGN3479 + mAb114 cocktail selection were infectious and resulted in the complete loss of mAb114 neutralization activity. A single mutation (Q508R), also identified in previous studies,[28] was sufficient for complete resistance to ZMapp and the two competing individual neutralizing components (2G4 and 4G7). Importantly, no single individual escape mutation impacted the neutralization of the non-competing three mAb (REGN-EB3) or two mAb (mAb114 + REGN3479) combinations that target distinct and non-overlapping antibody epitopes.

DISCUSSION

The recent clinical success of mAb therapies for EBOV and SARS-CoV-2 clearly demonstrates that antibody therapeutics targeting viral proteins offer a valuable option for both treatment and prophylaxis of viral infections.[2,33,34] Although vaccination will always be a critical component of the public health response to infectious agents, it is clear that a significant portion of the population will remain vulnerable to severe outcomes due to suboptimal responses to vaccines or challenges associated with vaccine access or uptake. Mass vaccination campaigns for infectious agents like EBOV may never occur, necessitating the availability of therapeutics in the event of disease outbreaks that are unpredictable in timing and location. Antibody-based therapeutics may offer additional protection from severe disease and death even to vaccinated individuals that fall into high-risk categories. Thus, antibody therapies that can be rapidly deployed can provide immediate treatment and protect recipients until vaccination and its associated immune response can mount. Indeed, 25% of PALM trial participants who experienced some level of EBOV disease reported that they had been vaccinated before the onset of symptoms.[2]

Protection against EBOV infection by an antibody cocktail can be achieved by combining complementary activities, including both neutralizing and Fc-recruiting functions.[9,10] REGN-EB3 combines individual mAbs with neutralizing (REGN3479 and REGN3470) and Fc-recruiting (REGN3470 and REGN3471) functions. Importantly, this cocktail contains antibodies with non-overlapping footprints; the distinction of the contact residues limits the likelihood of treatment-induced drug resistance.

Here, we present the cryo-EM structure at 3.1 Å resolution of the complete REGN3470, REGN3471, and REGN3479 cocktail bound to EBOV GP. Asymmetric reconstruction revealed eight Fab fragments simultaneously bound to the GP trimer: three each of REGN3479 and REGN3471 and two copies of REGN3470 in the final high-resolution model.

We are not aware of any published EBOV GP structure bound to antibodies that have been resolved to this resolution or better using asymmetric reconstruction of cryo-EM data. The ordering of this ~600 kDa complex and the binding of the REGN3470 antibody contained within it allow modeling key portions of the glycan cap, including the β17-β18 strands and the 27-residue loop in between. These sections were either fully disordered or only visible as main-chain tubes of indiscernible direction in previous crystal or cryo-EM structures. Here, they have been built in entirety, with visible side chains to confirm sequence and chain directionality. This model now corrects the direction of the chain in a previous high-resolution model in which density in this region was still unclear.

This cryo-EM structure further reveals the contents and key contacts contained within the three non-overlapping footprints of the component members of the cocktail. REGN3479 binds to a quaternary epitope bridging the fusion loop tip and paddle of one GP monomer to both GP1 and GP2 of the neighboring monomer. One key mechanism of action is by locking the GP in the pre-fusion conformation, similar to other fusion loop binding antibodies like ADI-15878,[20] and indeed, the epitope recognized by REGN3479 almost completely overlaps with that of ADI-15878. Ten of the 15 GP residues that interact with REGN3479 are shared with ADI-15878, and both antibodies recognize the conserved N-terminal pocket while displacing the non-conserved N terminus of GP2. However, only REGN3479 also contacts GP2 $HR1_A$. A second difference is that REGN3479 binds only the glycan itself, whereas ADI-15878 also binds the Asn side chain to which the glycan is linked.

Antibodies binding overlapping epitopes can have very different neutralization potentials that are hard to reconcile without high-resolution structures. For example, the general footprint and the overall vertical position of non-neutralizing REGN3471 resemble those of mAb114,[26] a potently neutralizing therapeutic antibody used as a monotherapy. A patch of hydrophobic residues in REGN3471 binds into the RBS underneath the hydrophilic crest of the GP (Figure 3D, left). By contrast, in mAb114, two arginines (Arg30 and Arg97) potentially form strong salt-bridging interactions with the GP crest residues Glu231 and Glu235, respectively (Figure 3D, right). Further, REGN3471 interacts with eight residues of the glycan cap while mAb114 interacts with only four. The greater dependence on glycan cap residues for binding likely explains why mAb114 exhibits higher affinity binding than REGN3471 to EBOV-GPcl and greater neutralization potency. The similarity of footprints and HCs utilized by these two antibodies demonstrates that Velocimmune mice can generate nearly identical antibody responses to humans.[35,36]

Fc-mediated immune effector functions play an important role in *in vivo* protection.[9] The existence and strength of these functions are controlled by antibody binding angle and accessibility of the Fc region to the respective Fc receptors. Although each of the antibodies in the REGN-EB3 cocktail have identical Fc domains, only REGN3470 and REGN3471

show potent immune effector functions—REGN3479, which binds to the side instead of the top of GP, has none.[13] REGN3470 binds radially outward from the top of the GP structure, anchoring solely to the glycan cap. REGN3471 binds vertically upward, anchoring into the RBS of EBOV GP and bridging it to the glycan cap. When homology models of REGN3470, REGN3471, and REGN3479 IgGs and a crystal structure of the receptor FcγR-IIIa bound to an IgG are docked into the cryo-EM map, it is evident that the Fc regions of REGN3470 and REGN3471 are easily accessible for FcγR-IIIa receptor binding while the Fc region of REGN3479 has limited accessibility (Figure S6A).

A key desired characteristic of any antiviral therapy is the minimal likelihood of drug-induced resistance, both in the treated individual and in the population in which a mutant virus may spread. With antibody therapeutics, these concerns may be especially great as mAb-induced mutations may also impact vaccine efficacy since these mutations may occur in epitopes recognized by endogenous polyclonal antibody responses as well. Although the risk of drug resistance cannot be fully eliminated, it can be greatly reduced with combination approaches. We have previously assessed the generation of viral resistance to SARS-CoV-2 spike antibody monotherapies and combinations and demonstrated that resistant viruses were rapidly selected with monotherapies and overlapping-epitope combinations, regardless of epitope conservation.[16,18] By contrast, the use of antibody combinations binding distinct epitopes reduced the risk of rapid viral escape by requiring concurrent selection of resistance mutations to each antibody.[37,38] Importantly, these findings based on surrogate *in vitro* escape studies were subsequently confirmed in real-world clinical data in COVID patients, validating the surrogate system as a relevant predictor of clinical resistance risk.[37,38]

In this study, we analyzed the ability of antibodies targeting diverse epitopes in the EBOV GP to prevent viral resistance, evaluated alone as monotherapies or when combined into different cocktails. As we observed with SARS-CoV-2, all neutralizing antibodies used as monotherapy lead to the rapid selection of escaping virus, even those antibodies (mAb114 and REGN3479) targeting conserved epitopes and thus predicted to be resistant to mutational escape.[39] Further, we observed that combinations of antibodies against overlapping epitopes also lead to the rapid selection of resistant viruses. By contrast, cocktails of antibodies against non-overlapping epitopes greatly reduced the likelihood of viral escape, whether composed of two (REGN3479 + mAb114) or three (REGN-EB3) mAb components, by requiring multiple mutations blocking the binding of each individual antibody for resistance. Similarly to SARS-CoV-2, the VSV-GP surrogate escape assay used in this study has identified *bona fide* variants associated with drug resistance of authentic EBOV *in vivo*. The variant observed under ZMapp selection in this escape assay (Q508R) was also identified in an EBOV-infected cynomolgus macaque that succumbed to the virus after ZMapp therapy.[28] Similar to SARS-CoV-2 spike mAb therapeutics, we were able to show that combination therapy against EBOV greatly reduces the risk of virus escape *in vitro*. Although challenging to obtain, further sequencing of samples from Ebola-infected patients treated with antibody therapeutics would be required to determine the incidence of drug resistance in the clinic.

In summary, the combined structural and functional analysis here reveals the footprints and key contacts of an FDA-approved therapeutic effective against EVD. It also demonstrates

that cocktails of antibodies targeting non-overlapping epitopes are key to mitigating the risk of drug-induced viral resistance.

STAR★METHODS

RESOURCE AVAILABILITY

Lead Contact—Further information requests should be directed to the lead contact Erica Ollmann Saphire (erica@lji.org).

Materials availability—All reagent requests in this study should be directed to the lead contact Erica Ollmann Saphire (erica@lji.org). Requests for REGN3479, REGN3471 and REGN3470 should be directed to Christos Kyratsous (christos.kyratsous@regeneron.com).

Data and code availability—The cryo-EM map has been deposited at the Electron Microscopy Data Bank (www.ebi.ac.uk/emdb). The accession number for the map is EMD-26005. The atomic model corresponding to the microscopy data has been deposited in the Protein Data Bank under the accession number PDB: 7TN9. No custom code was generated as part of the study.

Any additional information required to reanalyze the data reported in this work paper is available from the Lead Contact upon request.

EXPERIMENTAL MODEL AND SUBJECT DETAILS

Cell lines—HEK293T, Vero, Huh7, and BHK-21 cells were maintained in Dulbecco's Modified Eagle Medium (DMEM, Life Technologies), supplemented with 10% by volume heat inactivated Fetal Bovine Serum (FBS, Life Technologies), and 1% by volume Penicillin-Streptomycin-Glutamine (PSG, Life Technologies).

Drosophila Schneider S2 cells were grown in Schneider's Drosophila Medium at 27°C to generate stable cell lines. Insect-XPRESS protein-free medium with L-glutamine (Lonza) supplemented with puromycin (6 μg/mL) (InvivoGen) was used to grow S2 cells at 27°C for protein expression.

Viruses—The cloning and rescue of VSV-EBOV-GP is described below. Viral stocks were produced by infecting sub-confluent monolayers of BHK-21 at a multiplicity of infection (MOI) of 0.01. At 16-24 hours post infection, supernatants were collected and spun at 3000xg to remove cellular debris. Viral stocks were concentrated 25-fold by sucrose cushion ultracentrifugation, resuspended in Phosphate-buffered saline (PBS, Life Technologies), and frozen at −80 °C. Viral stocks were then titered by plaque assay on BHK-21 cells and sequence-confirmed by RNAseq (described below).

METHOD DETAILS

GP Expression and purification—Both mucin-containing and mucin-deleted EBOV GP were produced from stably transfected *Drosophila melanogaster* S2 cells. Briefly, Effectene (Qiagen) was used to transfect S2 cells with a modified pMT-puro vector plasmid containing the GP gene of interest. Transfected cells were selected by incubation at 27°C

for 4 weeks in complete Schneider's medium with 6μg/mL puromycin. The cells were then transitioned to Insect Xpress medium (Lonza) for large-scale expression in 2-liter Erlenmeyer flasks. Expression of secreted GP ectodomain was induced with 500 mM $CuSO_4$, and the supernatant was harvested after 5 days. The GP was engineered with a double Strep-tag at the C terminus to facilitate purification using a 5 mL Strep-trap HP column (GE) and then further purified by Superdex 200 size exclusion chromatography (SEC) in 50mM Tris-buffered saline (Tris-HCl, pH 7.5, 150mM NaCl [TBS]).

Cleavage and purification of REGN3470, REGN3471 and REGN3479 Fab fragments—To produce Fab fragments, each antibody (10mg) was digested with 200ɑg papain (5% w/w) for four hours at 37 °C; the reaction was quenched with 50mM iodoacetamide. The digested protein was dialyzed overnight at 4°C against 10mM Tris pH 8.0, 10mM NaCl buffer. The Fab fraction was then purified using a MonoQ 2mL column according to the manufacturer's protocol, followed by size exclusion chromatography using a Superdex 75 increase column equilibrated with 25mM Tris, 150mM NaCl, pH 7.5. The fractionated peak was concentrated in 10kDa MWCO Amicon Ultra 15 concentrators.

REGN3471 crystal screening, data collection and structure determination—Crystal screening of unbound Fab fragments of REGN3471 (6.6mg/mL) was performed using sparse matrix screens and an Oryx crystallization robot (Douglas instruments). Initial hits for crystals were obtained with 20% isopropyl alcohol, 20% PEG 4000, 100mM sodium citrate, pH 5.6. The crystals diffracted to 2.3Å at APS beamline 23-ID-B. The collected data were processed using XDS. Crystals were indexed in space group $P2_12_12_1$ and contained two Fabs in the asymmetric unit. Molecular replacement was used to iteratively determine phases. The initial molecular replacement model was generated by submitting the REGN3471 sequence to the SWISS-MODEL server41. Rebuilding and refinement were performed using Phenix and Coot. Molprobity and OMIT maps were used to validate model quality (Figure S1).

Preparation of GP-REGN-EB3 complex—To obtain complexes of GP with Inmazeb, GP (120μg) and the Fab fragments of REGN3470 (135μg), REGN3471 (125μg) and REGN3479 (150μg) were incubated together at room temperature overnight in a total volume of 500μL. The resulting complex was separated from excess Fabs using a Superose 6 Increase column equilibrated with 25mM Tris, 150mM NaCl, pH 7.5. Fractions containing the complex were combined and concentrated to 3.1mg/mL using a 100kDa MWCO Amicon concentrator.

Cryo-EM Sample preparation and data collection—C-flat™ EM (CF-2/1-4C-T, Electron Microscopy Sciences) grids were glow-discharged for 15 seconds on a Pelco Easiglow at 15nA power. The purified GP-REGN-EB3 complex (3μL, ~0.8mg/mL) was mixed with 1 μL 0.02mM lauryl maltose neopentyl glycol (LMNG) in 1X TBS and immediately applied to glow-discharged grids at 4 °C and 100% relative humidity inside a Vitrobot Mark IV. The grids were then blotted for 8 seconds without any extra applied blot force and plunge-frozen in liquid ethane. Frozen grids were imaged on a Thermo Fisher/Scientific Titan Krios (G3) equipped with a K2 direct electron detector and a

BioQuantum energy filter (Gatan) using SerialEM software. In initial efforts to freeze the GP-Fab complex onto grids, particles stuck to the grid hole edges, making data acquisition exceedingly difficult. Mixing the complex with the amphiphilic detergent Lauryl Maltose Neopentyl glycol (LMNG), immediately before freezing dramatically improved the observed particle count and enabled successful data collection. Three separate datasets were collected on separate days. A total of 6,360 movies were collected at 1.0504Å/pixel with 30 frames per movie and a dose of 33-52e^{-}/$Å^2$. Defocus targets cycled from −0.8 to −2.6 microns.

Cryo-EM map calculation, structure determination and structure refinement— All cryo-EM data processing was performed using cryoSPARC. Patch Motion correction and Patch CTF estimation were used to align and calculate the contrast transfer function (CTF), respectively. The cryoSPARC blob picking utility[19] was used to pick initial particles to develop a training data set of 3,154 particles that was fed into the Topaz particle picker[43] to yield 403,095 particles. The particle set was further 2D-classified to remove irrelevant particles. The resulting particle set was used for ab-initio reconstruction. Five ab initio classes were requested and all five classes were further subjected to heterogeneous refinement using all collected particles to generate representative 3D volumes. Of the five 3D volumes, two, containing 121,135 and 155,580 particles each, showed more promising features than the others (e.g., high-resolution features, antibody occupancy, and trimeric organization). One of these two 3D volumes contained two copies of REGN3470 Fab, whereas the other contained three copies, one of which is poorly ordered. The two particle sets combined yielded a final higher resolution map that contained two copies of REGN3470 and three copies each of REGN3471 and REGN3479. Hence, although the structure shows two copies, it is clear that complete occupancy is possible in solution. These two classes were combined in homogenous refinement followed by the final, non-uniform 3D refinement. All refinements were done with no symmetry explicitly applied (C1). The final refinement produced a 3.1Å map (using the Fourier shell correlation [FSC]=0.143 criterion) containing 276,715 particles. This map was further improved using DeepEMhancer,[44] a neural network-based density modification tool. Both the raw map and density-modified map were used to guide model building. A local resolution map is included as Figure S6B.

The GP-REGN-EB3 model was built by initially docking copies of the unbound REGN3471 Fab crystal structure and homology models of REGN3470 and REGN3479 generated using SWISS-MODEL,[41] and a published structure of GP (PDB 5JQ3). The EM density was clear for the Fv portions of the docked Fabs with unambiguous main-chain trace and conformation of all antibodies. Several rounds of Phenix[53] refinement, followed by manual rebuilding using Coot[54] yielded the final structure. Interacting residues of GP with the Fabs were selected using LigPlot+[47] and were further manually validated with interatomic distances <4Å for hydrogen bonds/salt bridges or hydrophobic surfaces with interatomic distances <5Å.

Structures were visualized and analyzed using UCSF Chimera[48] and UCSF ChimeraX.[49] Publication figures were made using Inkscape [https://inkscape.org]

BIAcore surface plasmon resonance analysis—Binding kinetics and affinities for each antibody in the REGN-EB3 cocktail and for mAb114 were individually assessed using surface plasmon resonance (SPR) technology on a Biacore T200 instrument (Cytiva, Marlborough, MA) using a Series S CM5 sensor chip in filtered and degassed HBS-EP running buffer (10 mM HEPES, 150 mM NaCl, 3mM EDTA, 0.05% (v/v) polysorbate 20, pH 7.4). Capture sensor surfaces were prepared by covalently immobilizing a mouse anti-human Fc mAb (REGN2567) on the chip surface using the standard amine coupling chemistry, as reported previously.[55] Following surface activation, the remaining active carboxyl groups on the CM5 chip surface were blocked by injecting 1M ethanolamine, pH8.0 for 7 minutes. A typical resonance unit (RU) signal of ~11,000 RU was achieved after the immobilization procedure.

Analysis of REGN3479, REGN3471, REGN3470 or mAb114 binding to EBOV-GP-DTM, and EBOV GP lacking the MLD (EBOV-GP-Δmuc) or glycan cap (glycan cap removed-EBOV-GP-Dmuc) was carried out by capturing the antibodies over immobilized anti-human Fc surface at 37°C. Following the capture of the antibodies, different concentrations of EBOV-GP proteins (6.25nM-200nM, two-fold serial dilution in duplicate) in the running buffer were injected for 2.5 minutes at a flow rate of 50μL/min with an 8-minute dissociation phase. At the end of each cycle, the anti-human Fc surface was regenerated using a 12-second injection of 20mM phosphoric acid.

Thermolysin cleavage studies—GP (2μg) was mixed with 2.25μg of each antibody separately and incubated at RT overnight before ~2μg of the complex was treated with 0.5μg Thermolysin L for 1 hour. Aliquots of the reaction were taken at indicated time points and quickly quenched with 5mM EDTA final concentration. Samples from each time point were evaluated by SDS-PAGE and western blotting.

Size-exclusion chromatography—GPcl (50 μg) was used to make a complex with equal amounts of each of the antibodies in REGN-EB3 individually. Mixtures were incubated for 4hrs at room temperature and run on S200i size exclusion column (Cytiva) equilibrated with 25mM Tris-base, 150mM NaCl pH 7.5 to monitor complex formation. Uncleaved GP (GP) and GPcl alone were also separately run on the S200i column as controls.

VSV-EBOV-GP generation—Fully replicative VSV-EBOV-GP was generated as previously described (Lawson, Rose/Whitt, Baum). In short, full-length North Kivu EBOV GP (GenBank accession MK007329.1) was cloned in place of VSV-G in a T7 promoter-driven VSV rescue plasmid. This genomic clone and the required expression plasmids for virus rescue (VSV-N, VSV-P, VSV-L, T7 polymerase) were transfected into HEK293T cells for 48 hours. The transfected cells were then co-cultured with BHK-21 cells transfected with VSV-G using the SE cell Line 4D-Nucleofector X Kit L (Lonza) and cultured until virus-mediated CPE was observed. The recovered virus was then plaque-purified twice to isolate individual clones.

Escape studies—VSV-EBOV-GP studies were performed as described for VSV-SARS-CoV-2-spike with minor modifications.[16] Briefly, 1.25 x 10^6 pfu of VSV-EBOV-GP was

incubated with serial dilutions of antibodies at room temperature for 30 minutes, and then used to infect 2.5 x 10^5 Vero cells (ATCC: CCL-81). The cells were then monitored for virus replication (CPE) for four days. Once the majority of cells displayed CPE, the supernatants were collected and frozen at −80 °C. Total RNA was extracted using TRIzol (Life Technologies) from the cell population and subjected to RNAseq to identify variants in the EBOV-GP protein. Each subsequent passage was performed by incubating 100μL of the supernatant under the same or higher antibody concentration until resistance to ≥ 10μg/mL antibody selection was observed in at least one passage or up to 10 passages.

Virus RNA Sequencing—RNA was quantified using the Qubit RNA HS Assay Kit (ThermoFisher). 1 to 50 ng RNA was treated by FastSelect-rRNAHMR(Qiagen) to remove host rRNA, and the incubation condition for fragmentation was followed as 85°C for 6 minutes, 75°C for 2 minutes, 70°C for 2 minutes, 65°C for 2 minutes, 60°C for 2 minutes, 55°C for 2 minutes, 37°C for 5 minutes, 25°C for 5 minutes, and hold at 4°C. Strand-specific RNA-seq libraries were prepared from the treated RNA using KAPA RNA HyperPrep Kit (Roche Sequencing). UDI with UMI Adapters (IDT) were ligated. Sixteen-cycle PCR was performed to amplify libraries. Sequencing was run on MiSeq (Illumina) by multiplexed paired-read run with 2X70 cycles.

VSV-EBOV-GP neutralization assays—Neutralization assays with the fully replicative VSV-EBOV-GP were performed by incubating 2,000 pfu of virus with serial dilutions of antibody starting at a concentration of 100μg/mL. The virus/antibody mixture was incubated at room temperature for 30 minutes and used to infect 2.0 x 10^4 Vero cells at an MOI of 0.1. At 24 hours post-infection, cells were fixed with 2% paraformaldehyde and permeabilized with 0.1 % Triton-X100. VSV-EBOV-GP infected cells were immunostained with a polyclonal rabbit anti-VSV serum (Imanis Life Sciences) that recognizes internal VSV proteins and an Alexa Fluor® 488 secondary antibody. Plate scans were imaged on a Cellular Technology Limited ImmunoSpot analyzer and fluorescent focus units (ffu) were determined using a SpectraMax i3 plate reader.

Growth of Filoviruses—Filoviruses were grown on Vero E6 cells (ATCC, VA). Viral supernatants were harvested from tissue culture media and stored at −80°C before use. Titers were determined by TCID50 (EBOV, RESTV, BDBV, SUDV) or by FFU (MARV) assays in Vero E6 cells. For TCID50, plates were monitored for CPE and fixed 5 to 7 days post infection. TCID50 values were calculated using the Reed-Muench method.[56] For FFU assay, cells were infected for approximately 48 hours, fixed in 10% formalin, and prepared for antibody staining. The cells were permeabilized in 0.1% Triton X-100, washed, and blocked in 3.5% BSA. Infected cells were then stained with a polyclonal anti-MARV VLP antibody (IBT Bioservices 04-0005) and an AF488-conjugated goat anti-rabbit secondary antibody. Plates were imaged on a Cytation 1 Multimode Plate Reader.

Filovirus neutralization assays—Antibodies were diluted into culture medium containing 10% fetal bovine serum and incubated with virus for 1 hour at 37°C. Antibody concentrations ranged from 20 μg/ml to 0.5 pg/ml. The mixture was added to Vero E6 cells for 48 hours. Following incubation, cells were fixed in 10% neutral buffered

formalin and virus was detected using smiFISH as previously described.[57] Briefly, cells were permeabilized with 70% ethanol and fixed with 15% formamide. Infected cells were detected with oligonucleotides targeting viral mRNAs from each filovirus and a fluorescently labeled (Cy5) detection probe (Integrated DNA Technologies). Images were acquired on a Nikon Ti2 using a 10X lens in DAPI and Cy5 channels. Images were processed using a CellProfiler pipeline to quantify nuclear staining intensity and mRNA intensity for each image. Infection was quantified as viral mRNA intensity normalized to nuclear intensity for each well, and this was further normalized to the average of infection values from wells treated with the lowest dilution of antibody.

Pseudoparticle generation—EBOV GP pseudoparticles (EBOVpp) were generated as described.[13] HEK293T cells were transfected with expression plasmids carrying the 2014 Zaire EBOV GP (KJ660346), lentivirus capsid proteins, and a lentivirus genome encoding a firefly luciferase under the control of the retrovirus long terminal repeat promoter. Supernatants were collected 48 hours post-transfection, clarified by centrifugation, and stored at −80 °C. Individual variants were cloned into 2014 Zaire EBOV GP (KJ660346) using site-directed mutagenesis and pseudotyped as described above.

Pseudoparticle neutralization assays—Pseudoparticle neutralization assays were performed by incubating EBOV pseudoparticles with serial dilutions of the indicated antibody. After 1 hour, the VLP/antibody mixtures were added to resuspended Huh7 (JCRB Cell Bank) and incubated for 72 hours. Luciferase signal from the lentivirus reporter was detected using a BrightGlo luciferase assay kit (Promega) and a Victor X3 plate reader (PerkinElmer).

QUANTIFICATION AND STATISTICAL ANALYSIS

NGS data analysis—NGS analysis was perform using Array Studio software package platform (Omicsoft). Quality of paired-end RNA Illumina reads was assessed using the ‘‘raw data QC of RNA-Seq data suite’’. Minimum and maximum read length, total nucleotide number, and GC% were calculated. Overall quality report was generated summarizing the quality of all reads in each sample, along each base pair. Paired-end RNA Illumina reads were then mapped against VSV-EBOV-GP virus genome using Omicsoft Sequence Aligner (OSA) version 4. Reads were trimmed by quality score using default parameters (when aligner encountered nucleotide in the read with a quality score of 2 or less, it trimmed the remainder of the read). OSA outputs were analyzed and annotated using Summarize Variant Data and Annotate Variant Data packages (Omicsoft). Target coverage was calculated for each sample. SNPs calling was performed using samples with average target coverage greater than 500 reads. SNPs with a minimum frequency of 1% and a coverage greater than 50 were identified and annotated.

SPR analysis—All specific SPR binding sensorgrams were double-reference subtracted as reported previously[58] and the kinetic parameters were obtained by globally fitting the double-reference subtracted data to a 1:1 binding model with mass transport limitation using Biacore T200 Evaluation software v3.1 (Cytiva). The dissociation rate constant (k_d) was determined by fitting the change in the binding response during the dissociation phase

and the association rate constant (k_a) was determined by globally fitting analyte binding at different concentrations. The equilibrium dissociation constant (K_D) was calculated from the ratio of k_d to k_a. The dissociative half-life ($t_{½}$) in minutes was calculated as ln2/(k_d*60).

Supplementary Material

Refer to Web version on PubMed Central for supplementary material.

ACKNOWLEDGMENTS

We gratefully acknowledge support from NIAID U19 AI142790, the Consortium for Immunotherapeutics against Emerging Viral Threats (E.O.S.), and the U.S. Department of Health and Health Services contract no. HHSO100201700016C (Regeneron). A portion of this project has been funded in part with federal funds from the Department of Health and Human Services, Office of the Assistant Secretary for Preparedness and Response, Biomedical Advanced Research and Development Authority, under OT number HHSO100201700020C. GM/CA@APS-23ID-B has been funded by the National Cancer Institute (ACB-12002) and the National Institute of General Medical Sciences (AGM-12006, P30GM138396). This research used resources of the Advanced Photon Source, a U.S. Department of Energy (DOE) Office of Science User Facility operated for the DOE Office of Science by Argonne National Laboratory under contract no. DE-AC02-06CH11357. The Eiger 16M detector at GM/CA-XSD was funded by NIH grant S10 OD012289. Cryo-EM SPA datasets were collected at Arizona State University. We acknowledge the use of facilities within the Eyring Materials Center at Arizona State University supported in part by NNCI-ECCS-1542160. We would like to acknowledge Dr. Dewight Williams from the Eyring Materials Center at Arizona State University supported in part by NNCI-ECCS-1542160 for assisting in data collection. We thank all the staff of the NIH who supported this study, in particular, Kaleb Sharer, Russel Byrum, Jennifer Jackson, Sarah Klim, Danny Ragland, Marisa St Claire, and Lisa Hensley. The authors would like to thank Kristen Tramaglini for her continuous support with this project.

INCLUSION AND DIVERSITY

One or more of the authors of this paper self-identifies as a gender minority in their field of research. While citing references scientifically relevant for this work, we also actively worked to promote gender balance in our reference list.

REFERENCES

1. Pratt C. (2020). Two Ebola virus variants circulating during the 2020 Equateur Province outbreak. https://virological.org/t/two-ebola-virus-variants-circulating-during-the-2020-equateur-province-outbreak/538.
2. Mulangu S, Dodd LE, Davey RT Jr., Tshiani Mbaya O, Proschan M, Mukadi D, Lusakibanza Manzo M, Nzolo D, Tshomba Oloma A, Ibanda A, et al. (2019). A randomized, controlled trial of Ebola virus disease therapeutics. N. Engl. J. Med 381, 2293–2303. 10.1056/NEJMoa1910993. [PubMed: 31774950]
3. Center for Drug Evaluation and Research (2020). FDA approves treatment for Ebola virus (U.S. Food and Drug Administration). https://www.fda.gov/drugs/news-events-human-drugs/fda-approves-treatment-ebola-virus.
4. Sanchez A, Yang ZY, Xu L, Nabel GJ, Crews T, and Peters CJ (1998). Biochemical analysis of the secreted and virion glycoproteins of Ebola virus. J. Virol 72, 6442–6447. 10.1128/JVI.72.8.6442-6447.1998. [PubMed: 9658086]
5. Lee JE, Fusco ML, Hessell AJ, Oswald WB, Burton DR, and Saphire EO (2008). Structure of the Ebola virus glycoprotein bound to an antibody from a human survivor. Nature 454, 177–182. 10.1038/nature07082. [PubMed: 18615077]
6. Wang H, Shi Y, Song J, Qi J, Lu G, Yan J, and Gao GF (2016). Ebola viral glycoprotein bound to its endosomal receptor Niemann-Pick C1. Cell 164, 258–268. 10.1016/j.cell.2015.12.044. [PubMed: 26771495]

7. Gregory SM, Harada E, Liang B, Delos SE, White JM, and Tamm LK (2011). Structure and function of the complete internal fusion loop from Ebolavirus glycoprotein 2. Proc. Natl. Acad. Sci. USA 108, 11211–11216. 10.1073/pnas.1104760108. [PubMed: 21690393]
8. Ito H, Watanabe S, Takada A, and Kawaoka Y (2001). Ebola virus glycoprotein: proteolytic processing, acylation, cell tropism, and detection of neutralizing antibodies. J. Virol 75, 1576–1580. 10.1128/JVI.75.3.1576-1580.2001. [PubMed: 11152533]
9. Saphire EO, Schendel SL, Fusco ML, Gangavarapu K, Gunn BM, Wec AZ, Halfmann PJ, Brannan JM, Herbert AS, Qiu X, et al. (2018). Systematic analysis of monoclonal antibodies against Ebola virus GP defines features that contribute to protection. Cell 174. 938–952. e13. 10.1016/j.cell.2018.07.033. [PubMed: 30096313]
10. Gunn BM, Yu WH, Karim MM, Brannan JM, Herbert AS, Wec AZ, Halfmann PJ, Fusco ML, Schendel SL, Gangavarapu K, et al. (2018). A role for Fc function in therapeutic monoclonal antibody-mediated protection against Ebola virus. Cell Host Microbe 24. 221–233. e5. 10.1016/j.chom.2018.07.009. [PubMed: 30092199]
11. Gilchuk P, Murin CD, Milligan JC, Cross RW, Mire CE, Ilinykh PA, Huang K, Kuzmina N, Altman PX, Hui S, et al. (2020). Analysis of a therapeutic antibody cocktail reveals determinants for cooperative and broad Ebolavirus neutralization. Immunity 52. 388–403.e12. 10.1016/j.immuni.2020.01.001. [PubMed: 32023489]
12. Qiu X, Wong G, Audet J, Bello A, Fernando L, Alimonti JB, Fausther-Bovendo H, Wei H, Aviles J, Hiatt E, et al. (2014). Reversion of advanced Ebola virus disease in nonhuman primates with ZMapp. Nature 514, 47–53. 10.1038/nature13777. [PubMed: 25171469]
13. Pascal KE, Dudgeon D, Trefry JC, Anantpadma M, Sakurai Y, Murin CD, Turner HL, Fairhurst J, Torres M, Rafique A, et al. (2018). Development of clinical-stage human monoclonal antibodies that treat advanced Ebola virus disease in nonhuman primates. J. Infect. Dis 218, S612–S626. 10.1093/infdis/jiy285. [PubMed: 29860496]
14. De Clercq E, and Li G (2016). Approved antiviral drugs over the past 50 years. Clin. Microbiol. Rev 29, 695–747. 10.1128/CMR.00102-15. [PubMed: 27281742]
15. Misasi J, and Sullivan NJ (2021). Immunotherapeutic strategies to target vulnerabilities in the Ebolavirus glycoprotein. Immunity 54, 412–436. 10.1016/j.immuni.2021.01.015. [PubMed: 33691133]
16. Copin R, Baum A, Wloga E, Pascal KE, Giordano S, Fulton BO, Zhou A, Negron N, Lanza K, Chan N, et al. (2021). The monoclonal antibody combination REGEN-COV protects against SARS-CoV-2 mutational escape in preclinical and human studies. Cell 184. 3949–3961. e11. 10.1016/j.cell.2021.06.002. [PubMed: 34161776]
17. Rockett RJ, Basile K, Maddocks S, Fong W, Agius JE, Mackinnon JJ, Arnott A, Chandra S, Gall M, Draper J, et al. (2021). Resistance conferring mutations in SARS-CoV-2 delta following sotrovimab infusion. N. Engl. J. Med 386, 1477–1479. 10.1056/NEJMc2120219.
18. Baum A, Fulton BO, Wloga E, Copin R, Pascal KE, Russo V, Giordano S, Lanza K, Negron N, Ni M, et al. (2020). Antibody cocktail to SARS-CoV-2 spike protein prevents rapid mutational escape seen with individual antibodies. Science 369, 1014–1018. 10.1126/science.abd0831. [PubMed: 32540904]
19. Punjani A, Rubinstein JL, Fleet DJ, and Brubaker MA (2017). cryoSPARC: algorithms for rapid unsupervised cryo-EM structure determination. Nat. Methods 14, 290–296. 10.1038/nmeth.4169. [PubMed: 28165473]
20. West BR, Moyer CL, King LB, Fusco ML, Milligan JC, Hui S, and Saphire EO (2018). Structural basis of pan-Ebolavirus neutralization by a human antibody against a conserved, yet cryptic epitope. mBio 9. e01674–18. 10.1128/mBio.01674-18. [PubMed: 30206174]
21. Gregory SM, Larsson P, Nelson EA, Kasson PM, White JM, and Tamm LK (2014). Ebolavirus entry requires a compact hydrophobic fist at the tip of the fusion loop. J. Virol 88, 6636–6649. 10.1128/JVI.00396-14. [PubMed: 24696482]
22. Chandran K, Sullivan NJ, Felbor U, Whelan SP, and Cunningham JM (2005). Endosomal proteolysis of the Ebola virus glycoprotein is necessary for infection. Science 308, 1643–1645. 10.1126/science.1110656. [PubMed: 15831716]

23. Brecher M, Schornberg KL, Delos SE, Fusco ML, Saphire EO, and White JM (2012). Cathepsin cleavage potentiates the Ebola virus glycoprotein to undergo a subsequent fusion-relevant conformational change. J. Virol 86, 364–372. 10.1128/JVI.05708-11. [PubMed: 22031933]
24. Marzi A, Reinheckel T, and Feldmann H (2012). Cathepsin B & L are not required for Ebola virus replication. PLoS Negl. Trop. Dis 6, e1923. 10.1371/journal.pntd.0001923. [PubMed: 23236527]
25. Misasi J, Chandran K, Yang JY, Considine B, Filone CM, Côté M, Sullivan N, Fabozzi G, Hensley L, and Cunningham J (2012). Filoviruses require endosomal cysteine proteases for entry but exhibit distinct protease preferences. J. Virol 86, 3284–3292. 10.1128/JVI.06346-11. [PubMed: 22238307]
26. Misasi J, Gilman MSA, Kanekiyo M, Gui M, Cagigi A, Mulangu S, Corti D, Ledgerwood JE, Lanzavecchia A, Cunningham J, et al. (2016). Structural and molecular basis for Ebola virus neutralization by protective human antibodies. Science 351, 1343–1346. 10.1126/science.aad6117. [PubMed: 26917592]
27. Saphire EO, Schendel SL, Gunn BM, Milligan JC, and Alter G (2018). Antibody-mediated protection against Ebola virus. Nat. Immunol 19, 1169–1178. 10.1038/s41590-018-0233-9. [PubMed: 30333617]
28. Qiu X, Audet J, Wong G, Pillet S, Bello A, Cabral T, Strong JE, Plummer F, Corbett CR, Alimonti JB, and Kobinger GP (2012). Successful treatment of Ebola virus-infected cynomolgus macaques with monoclonal antibodies. Sci. Transl. Med 4, 138ra81. 10.1126/scitranslmed.3003876.
29. Audet J, Wong G, Wang H, Lu G, Gao GF, Kobinger G, and Qiu X (2014). Molecular characterization of the monoclonal antibodies composing ZMAb: a protective cocktail against Ebola virus. Sci. Rep 4, 6881. 10.1038/srep06881. [PubMed: 25375093]
30. Davidson E, Bryan C, Fong RH, Barnes T, Pfaff JM, Mabila M, Rucker JB, and Doranz BJ (2015). Mechanism of binding to Ebola virus glycoprotein by the ZMapp, ZMAb, and MB-003 cocktail antibodies. J. Virol 89, 10982–10992. 10.1128/JVI.01490-15. [PubMed: 26311869]
31. Miller CR, Johnson EL, Burke AZ, Martin KP, Miura TA, Wichman HA, Brown CJ, and Ytreberg FM (2016). Initiating a watch list for Ebola virus antibody escape mutations. PeerJ 4, e1674. 10.7717/peerj.1674. [PubMed: 26925318]
32. Mbala-Kingebeni P, Aziza A, Di Paola N, Wiley MR, Makiala-Mandanda S, Caviness K, Pratt CB, Ladner JT, Kugelman JR, Prieto K, et al. (2019). Medical countermeasures during the 2018 Ebola virus disease outbreak in the North Kivu and Ituri Provinces of the Democratic Republic of the Congo: a rapid genomic assessment. Lancet Infect. Dis 19, 648–657. 10.1016/S1473-3099(19)30118-5. [PubMed: 31000464]
33. Weinreich DM, Sivapalasingam S, Norton T, Ali S, Gao H, Bhore R, Musser BJ, Soo Y, Rofail D, Im J, et al. (2021). REGN-COV2, a neutralizing antibody cocktail, in Outpatients with Covid-19. N. Engl. J. Med 384, 238–251. 10.1056/NEJMoa2035002. [PubMed: 33332778]
34. O'Brien MP, Forleo-Neto E, Musser BJ, Isa F, Chan K-C, Sarkar N, Bar KJ, Barnabas RV, Barouch DH, Cohen MS, et al. (2021). Subcutaneous REGEN-COV antibody combination to prevent Covid-19. N. Engl. J. Med 385, 1184–1195. 10.1056/NEJMoa2109682. [PubMed: 34347950]
35. Macdonald LE, Karow M, Stevens S, Auerbach W, Poueymirou WT, Yasenchak J, Frendewey D, Valenzuela DM, Giallourakis CC, Alt FW, et al. (2014). Precise and in situ genetic humanization of 6 Mb of mouse immunoglobulin genes. Proc. Natl. Acad. Sci. USA 111, 5147–5152. 10.1073/pnas.1323896111. [PubMed: 24706858]
36. Murphy AJ, Macdonald LE, Stevens S, Karow M, Dore AT, Pobursky K, Huang TT, Poueymirou WT, Esau L, Meola M, et al. (2014). Mice with megabase humanization of their immunoglobulin genes generate antibodies as efficiently as normal mice. Proc. Natl. Acad. Sci. USA 111, 5153–5158. 10.1073/pnas.1324022111. [PubMed: 24706856]
37. Rockett R, Basile K, Maddocks S, Fong W, Agius JE, Johnson-Mackinnon J, Arnott A, Chandra S, Gall M, Draper J, et al. (2022). Resistance mutations in SARS-CoV-2 delta variant after sotrovimab use. N. Engl. J. Med 386, 1477–1479. 10.1056/NEJMc2120219. [PubMed: 35263515]
38. Choudhary MC, Chew KW, Deo R, Flynn JP, Regan J, Crain CR, Moser C, Hughes M, Ritz J, Ribeiro RM, et al. (2021). Emergence of SARS-CoV-2 resistance with monoclonal antibody therapy. Preprint at medRxiv. 10.1101/2021.09.03.21263105.

39. Gaudinski MR, Coates EE, Novik L, Widge A, Houser KV, Burch E, Holman LA, Gordon IJ, Chen GL, Carter C, et al. (2019). Safety, tolerability, pharmacokinetics, and immunogenicity of the therapeutic monoclonal antibody mAb114 targeting Ebola virus glycoprotein (VRC 608): an open-label phase 1 study. Lancet 393, 889–898. 10.1016/S0140-6736(19)30036-4. [PubMed: 30686586]
40. Bunch TA, Grinblat Y, and Goldstein LS (1988). Characterization and use of the Drosophila metallothionein promoter in cultured *Drosophila melanogaster* cells. Nucleic Acids Res. 16, 1043–1061. 10.1093/nar/16.3.1043. [PubMed: 3125519]
41. Waterhouse A, Bertoni M, Bienert S, Studer G, Tauriello G, Gumienny R, Heer FT, de Beer TAP, Rempfer C, Bordoli L, et al. (2018). SWISS-MODEL: homology modelling of protein structures and complexes. Nucleic Acids Res. 46, W296–W303. 10.1093/nar/gky427. [PubMed: 29788355]
42. Mastronarde DN (2005). Automated electron microscope tomography using robust prediction of specimen movements. J. Struct. Biol 152, 36–51. 10.1016/j.jsb.2005.07.007. [PubMed: 16182563]
43. Bepler T, Morin A, Noble AJ, Brasch J, Shapiro L, and Berger B (2018). Positive-unlabeled convolutional neural networks for particle picking in cryo-electron micrographs. Res. Comput. Mol. Biol 10812, 245–247. [PubMed: 29707703]
44. Sanchez-Garcia R, Gomez-Blanco J, Cuervo A, Carazo JM, Sorzano COS, and Vargas J (2021). DeepEMhancer: a deep learning solution for cryo-EM volume post-processing. Commun. Biol 4, 874. 10.1038/s42003-021-02399-1. [PubMed: 34267316]
45. Adams PD, Afonine PV, Bunkóczi G, Chen VB, Davis IW, Echols N, et al. (2010). PHENIX: a comprehensive Python-based system for macromolecular structure solution. Acta Crystallogr. D Biol. Crystallogr 66, 213–221. 10.1107/S0907444909052925. [PubMed: 20124702]
46. Emsley P, and Cowtan K (2004). Coot: model-building tools for molecular graphics. Acta Crystallogr. D Biol. Crystallogr 60, 2126–2132. 10.1107/S0907444904019158. [PubMed: 15572765]
47. Laskowski RA, and Swindells MB (2011). LigPlot+: multiple ligand-protein interaction diagrams for drug discovery. J. Chem. Inf. Model 51, 2778–2786. 10.1021/ci200227u. [PubMed: 21919503]
48. Pettersen EF, Goddard TD, Huang CC, Couch GS, Greenblatt DM, Meng EC, and Ferrin TE (2004). UCSF Chimera–a visualization system for exploratory research and analysis. J. Comput. Chem 25, 1605–1612. 10.1002/jcc.20084. [PubMed: 15264254]
49. Pettersen EF, Goddard TD, Huang CC, Meng EC, Couch GS, Croll TI, Morris JH, and Ferrin TE (2021). UCSF ChimeraX: structure visualization for researchers, educators, and developers. Protein Sci. 30, 70–82. 10.1002/pro.3943. [PubMed: 32881101]
50. Website Inkscape Project, 2020. Inkscape, Available at: https://inkscape.org.
51. Williams CJ, Headd JJ, Moriarty NW, Prisant MG, Videau LL, Deis LN, et al. (2018). MolProbity: More and better reference data for improved all-atom structure validation. Protein Sci 27, 293–315. 10.1002/pro.3330. [PubMed: 29067766]
52. Terwilliger TC, Grosse-Kunstleve RW, Afonine PV, Moriarty NW, Zwart PH, Hung LW, et al. (2008). Iterative model building, structure refinement and density modification with the PHENIX AutoBuild wizard. Acta Crystallogr. D Biol. Crystallogr 64, 61–69. 10.1107/S090744490705024X. [PubMed: 18094468]
53. Liebschner D, Afonine PV, Baker ML, Bunkóczi G, Chen VB, Croll TI, Hintze B, Hung LW, Jain S, McCoy AJ, et al. (2019). Macromolecular structure determination using X-rays, neutrons and electrons: recent developments in Phenix. Acta Crystallogr. D Struct. Biol 75, 861–877. 10.1107/S2059798319011471. [PubMed: 31588918]
54. Emsley P, Lohkamp B, Scott WG, and Cowtan K (2010). Features and development of coot. Acta Crystallogr. D Biol. Crystallogr 66, 486–501. 10.1107/S0907444910007493. [PubMed: 20383002]
55. Johnsson B, Löfås S, and Lindquist G (1991). Immobilization of proteins to a carboxymethyldextran-modified gold surface for biospecific interaction analysis in surface plasmon resonance sensors. Anal. Biochem 198, 268–277. 10.1016/0003-2697(91)90424-r. [PubMed: 1724720]
56. Reed LJ, and Muench H (1938). A Simple Method for Estimating Fifty Per Cent Endpoints (Lancaster Press, Incorporated).

57. Tsanov N, Samacoits A, Chouaib R, Traboulsi A-M, Gostan T, Weber C, Zimmer C, Zibara K, Walter T, Peter M, et al. (2016). smiFISH and FISH-quant - a flexible single RNA detection approach with super-resolution capability. Nucleic Acids Res. 44, e165. 10.1093/nar/gkw784. [PubMed: 27599845]

58. Myszka DG (1999). Improving biosensor analysis. J. Mol. Recognit 12, 279–284. 10.1002/(SICI)1099-1352(199909/10)12:5<279::AID-JMR473>3.0.CO;2-3. [PubMed: 10556875]

Highlights

- Inmazeb antibody cocktail targets three discrete epitopes on Ebola virus GP trimer
- High-resolution structure maps in detail the three contact sites
- Inmazeb-GP structure defines GP glycan cap regions
- Unlike monotherapies, Inmazeb cocktail prevents rapid selection of drug-resistant virus

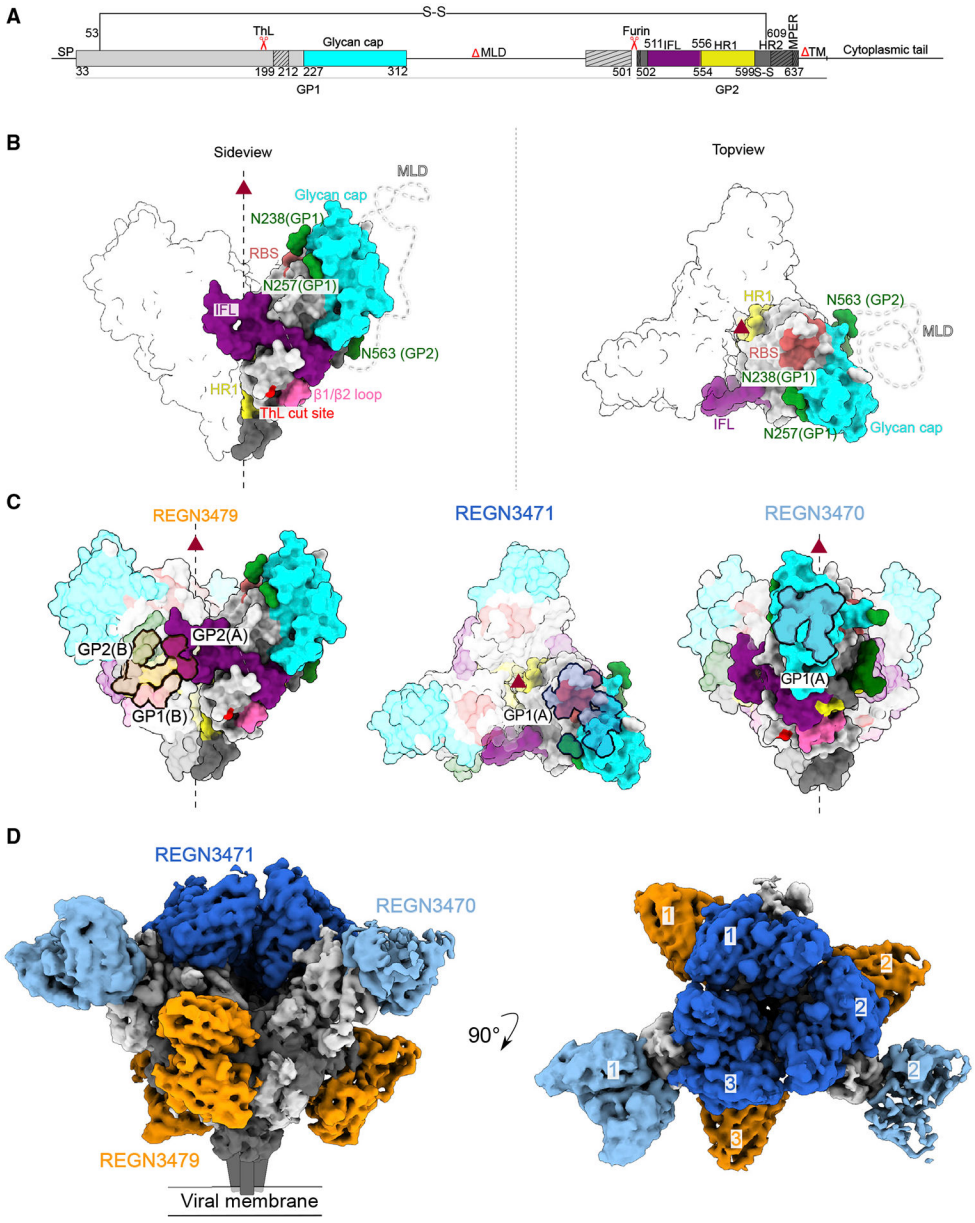

Figure 1. Structural overview of REGN-EB3 bound to EBOV GP

(A) Schematic representation of EBOV GP ectodomain. The mucin-like domain (MLD) and transmembrane (TM) domains are deleted. Thermolysin (ThL) and furin cleavage sites are indicated. A disulfide bond links the N-terminal portion of GP1 (light gray) to GP2 (dark gray). The glycan cap, internal fusion loop (IFL), and heptad repeats 1 (HR1) are colored cyan, purple, and yellow, respectively. Hash-marked regions in the schematic correspond to disordered regions in the structure.

(B) Surface representation of side and top views of the EBOV GP trimer in the complex. The dotted line indicates the approximate region of the MLD. The β1-β2 loop (pink), receptor-binding site (RBS; brick red), ThL cut site (red), glycan cap (cyan), mucin-like domain (MLD; white), internal fusion loop (IFL; purple), heptad repeat 1 (HR1; yellow), and glycans (green) are shown.

(C) Surface representation of EBOV GP trimer with each of the three different antibody footprints illustrated as a black outline in three separate views The dotted line and the red triangle indicated the 3-fold axis of the GP trimer.
(D) The 3.1 Å cryo-EM map of the EBOV GP bound to eight Fabs of the REGN-EB3 cocktail. GP1 and GP2 are light and dark gray, respectively. REGN3470, REGN3471, and REGN3479 are colored light blue, dark blue, and orange, respectively. The number of copies of each antibody bound simultaneously to the GP trimer is labeled.
See also Figures S1, S2, and S6 and Tables S1 and S2.

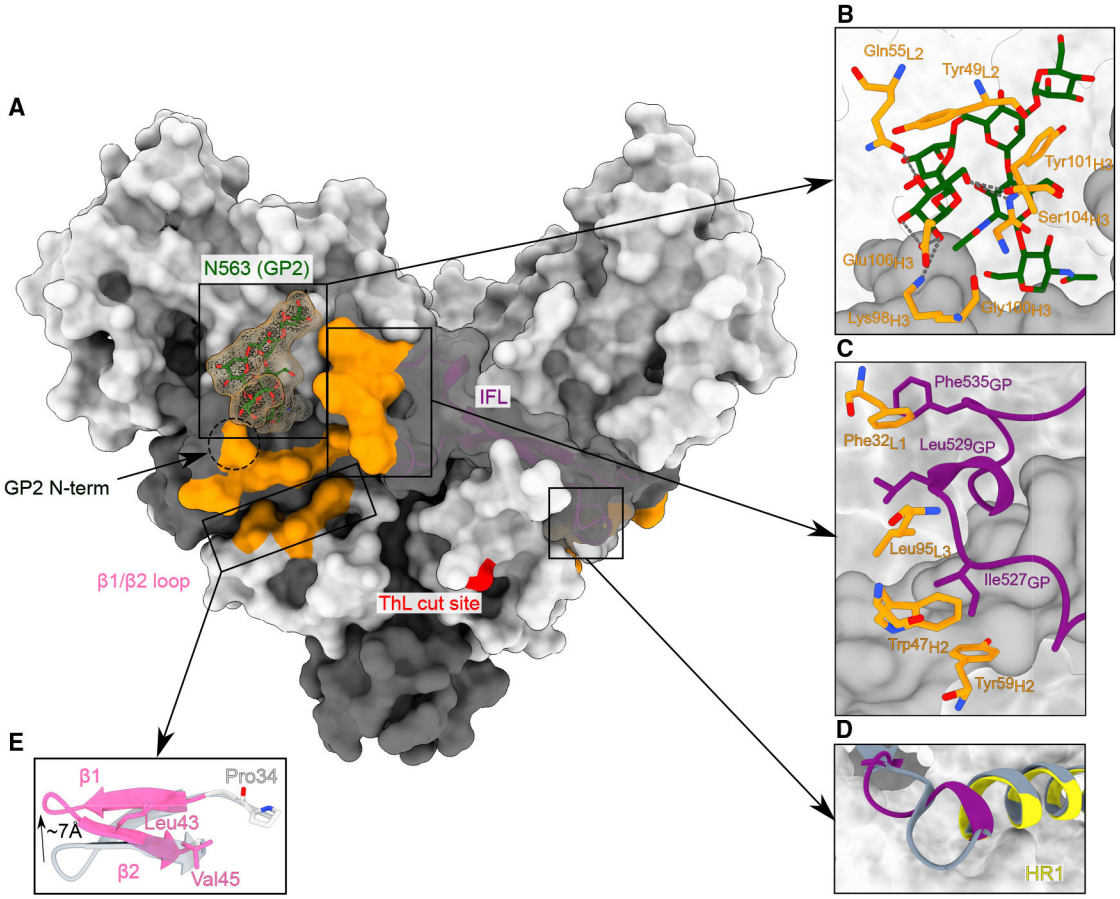

Figure 2. REGN3479 targets a quaternary epitope on the GP trimer

(A) Surface representation of the GP trimer with the REGN3479 epitope footprint colored in orange, glycan moieties are in green, and the thermolysin cleavage site is in red.

(B) REGN3479 residues (orange) interact extensively with the Asn563 glycan (green).

(C) REGN3479 interactions (orange) with the fusion loop (purple). LC residue Phe32 wedges into the fusion loop tip.

(D) Overlay GP (residues 547–554) in the unbound (gray, PDB ID:5JQ3) and REGN3479-bound form (purple) with the HR1 shown as a gray (unbound) and yellow (bound), respectively, ribbon diagram. Antibody binding introduces an additional helical turn in the HR1 N terminus (purple).

(E) The β1/β2 loop shifts by 7 Å in the unbound (gray) to bound (pink) shows an ~7 Å shift mediated by REGN3479 binding.

See also Table S3.

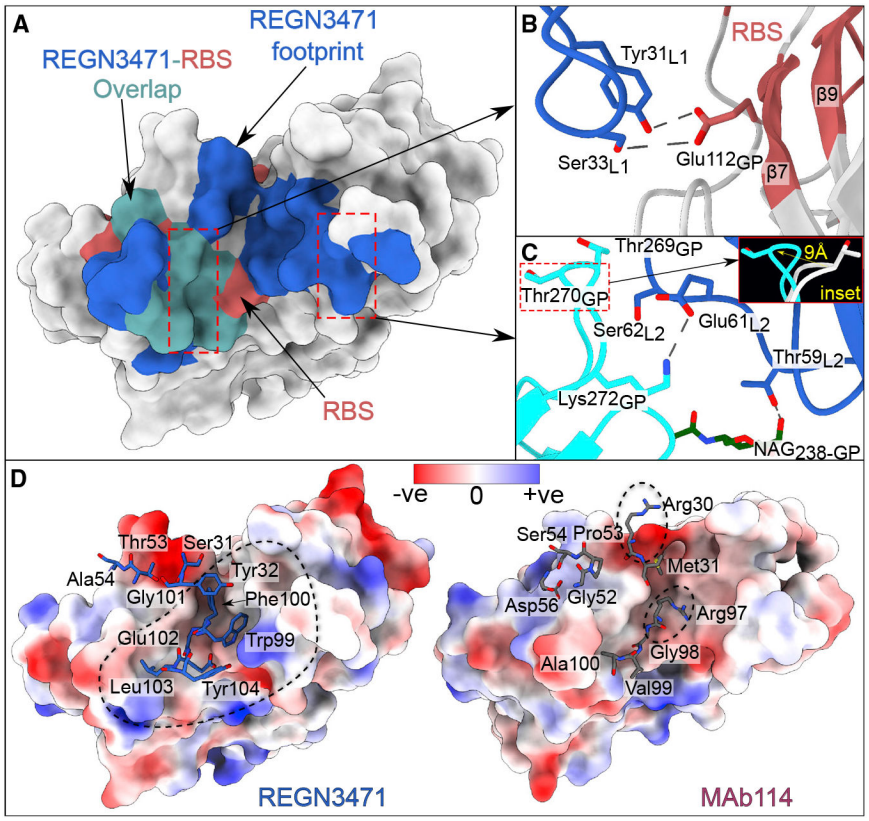

Figure 3. REGN3471 binds both the head and glycan cap of GP

(A) Top view of REGN3471 footprint shown in blue, receptor-binding site (RBS) in brick red. Residues that overlap between the REGN3471 footprint and RBS shown in teal.

(B) REGN3471 CDRL1 forms hydrogen bonds with residues in the hydrophilic, receptor-binding crest of GP.

(C) A salt-bridge interaction between Lys 272 of GP and Glu 61 of REGN3471 enhances antibody binding affinity. The inset shows the overlay of GP in unbound (gray, PDB ID:5JQ3) and bound (cyan) forms. Steric clashes with Ser62 of the Fab displace the GP Thr 270 by ~9 Å. Thr 270 loop movement is not observed with mAb114 binding.

(D) Electrostatic maps of GP bound to REGN3471 (left) or mAb114 (right). Antibody residues unique to REGN3471 or mAb114 are labeled. Several hydrophobic residues in REGN3471 occupy the hydrophilic crest of GP. Although the resolution of the mAb114 complex is low, stronger and more favorable hydrophilic residues of mAb114 relative to REGN3471 interact with the GP crest to form high-affinity salt bridges and also participate in other interactions.

See also Table S3.

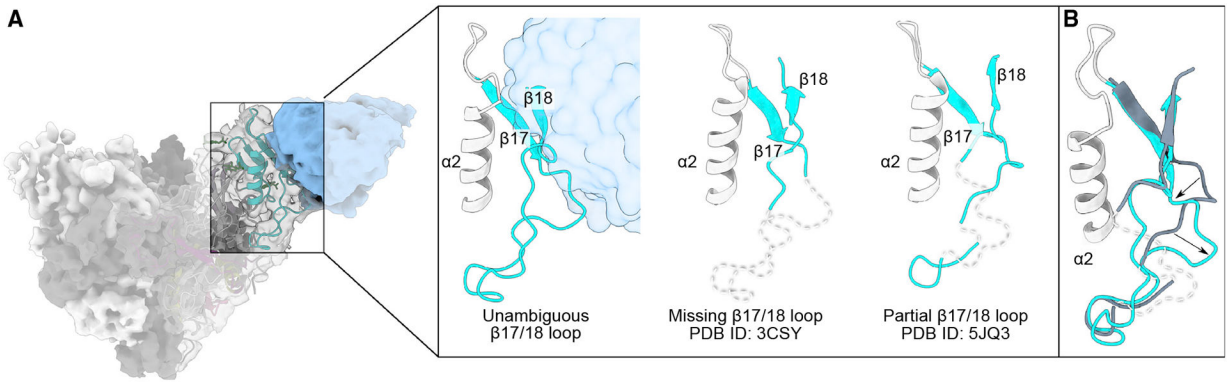

Figure 4. REGN3470 stabilizes the β17/β18 loop in the glycan cap

(A) Cryo-EM map of REGN3470 bound to EBOV GP. Inset compares the β17/18 loop in REGN3470 bound to GP and two previously published structures (PDB ID:3CSY and 5JQ3). The unambiguous density of this loop is observed in the REGN3470 complex.

(B) Comparison of unbound GP (PDB ID: 5JQ3, gray) with GP bound to REGN3470 shows the movement of the loop upon REGN3470 binding.

See also Table S3.

A

Antibody	EBOV-GP $k_a(M^{-1}s^{-1})$	$k_d(s^{-1})$	$K_D(M)$	$t_{1/2}$ (min)
REGN3479	6.61E+04	1.08E-04	1.64E-09	106.9
REGN3471	3.68E+04	1.63E-04	4.42E-09	70.9
REGN3470	7.95E+04	9.50E-05	1.19E-09	121.6
mAb114	9.84E+04	3.08E-05	3.13E-10	375
Antibody	EBOV-GPcl $k_a(M^{-1}s^{-1})$	$k_d(s^{-1})$	$K_D(M)$	$t_{1/2}$ (min)
REGN3479	7.26E+05	1.03E-04	1.42E-10	112.1
REGN3471	4.12E+04	6.50E-04	1.58E-08	17.8
REGN3470	NB	NB	NB	NB
mAb114	6.68E+05	1.38E-04	2.06E-10	83.7

Abbreviations: EBOV - Ebola virus; GP - glycoprotein; GPcl - glycoprotein cleaved; NB - no binding

B

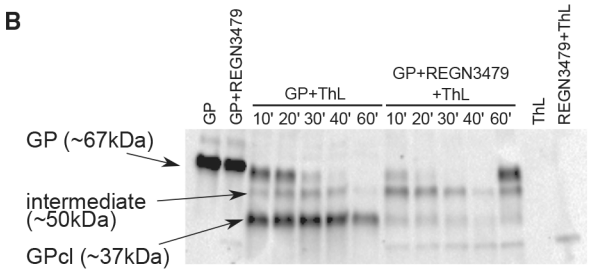

Figure 5. Glycan cap removal abolishes REGN3470 GP binding and reduces REGN3471 GP binding

(A) Ligand binding properties of REGN-EB3 cocktail antibodies. Summary of equilibrium dissociation constants (K_D) for the interaction of surface-captured anti-EBOV antibody with recombinant EBOV GP or GPCL trimer protein, respectively. k_a, association rate constant; k_d, dissociation rate constant; K_D, equilibrium dissociation constant; $t_{½}$, dissociative half-life.

(B) Time-dependent thermolysin cleavage of GP in the absence and presence of REGN3479. See Figures S3 and S4.

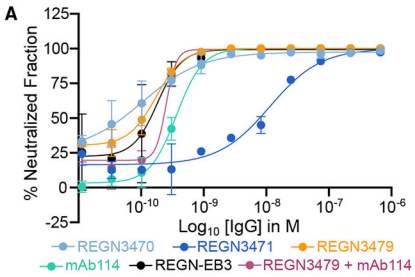

B

Antibody	VSV-EBOV-GP IC50
REGN3470	1.05E-10
REGN3471	1.14E-08
REGN3479	1.73E-10
mAb114	3.65E-10
REGN-EB3	1.83E-10
REGN3479+mAb114	2.51E-10
Isotype	Non-neutralizing

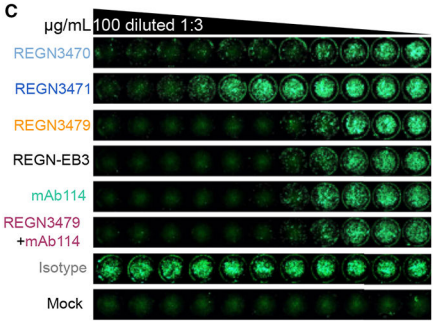

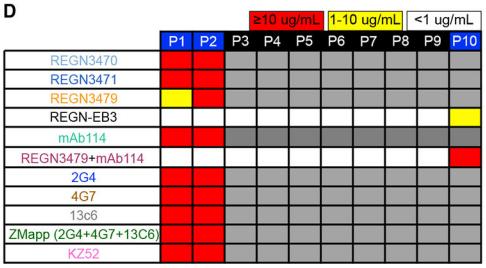

E

Antibody selection	Passage 1	Passage 2	Passage 10
REGN3470	E304A (7%)	E304A (22%)	Complete[b]
REGN3471	P34S (2%) T144M (2%) G224D (3%)	P34S (45%) P116H (2%) T144M (33%) G224D (88%)	Complete[b]
REGN3479	S347F (11%) G528R (96%)	S347F (28%) G528R (100%)	Complete
REGN-EB3	N.D.[a] (<10ug/mL)	N.D.[a] (<10ug/mL)	N.D.[a] (<10ug/mL)
mAb114	P116H (49%) G118R (18%) G118E (17%) T144M (5%)	P116H (63%) G118R (18%) G118E (9%)	Complete[b]
REGN3479+mAb114	N.D. (<10ug/mL)	N.D. (<10ug/mL)	G118R (3%) T144M (100%) T469I (99%) N563Y (100%)
2G4	Q508R (78%)	Q508R (95%)	Complete[b]
4G7	Q508R (4%) G557R (37%)	Q508R (18%) G557R (42%)	Complete[b]
13c6	No variants detected	No variants detected	Complete[b]
ZMapp (2G4+4G7+13C6)	Q508R (37%)	Q508R (80%)	Complete[b]
KZ52	Q508R (9%) G557R (64%)	Q508R (6%) G557R (89%)	Complete[b]

[a]N.D. = Not determined. No viral replication observed at high Ab concentrations (≥10ug/mL)
[b]Complete = Study over. At least one previous passage at high antibody concentration (≥10ug/mL)

Figure 6. REGN-EB3 prevents rapid viral escape

(A) Neutralization curves of fully replicative VSV-EBOV-GP by individual REGN-EB3 components, mAb114, a two-mAb combination (REGN3479 + mAb114), or the three-mAb REGN-EB3.

(B) IC50 values (in M).

(C) Images of representative plates.

(D) Selection of escape variants to individual mAbs and combinations. To identify escape variants, VSV-EBOV-GP was propagated under antibody pressure to select for the resistant virus. The maximal antibody concentration under which virus replication was observed for each passage is indicated: ≥10 µg/mL (red), 1–10 µg/mL (orange), and <1 µg/mL (white).

(E) Variants identified through RNA-seq under greater than ≥10 µg/mL of antibody selection. Values in parentheses are the relative frequency of reads encoding a given variant

among all reads in that position. N.D., not determined, as no viral replication was observed at high mAb concentration (≥ 10 μg/mL). Complete: at least one previous passage at high antibody concentration (≥10 μg/mL).
See also Figures S4 and S5.

Table 1.

Fold-decrease in potency relative to wild-type (WT) pseudovirus

	REGN3479	REGN-EB3	mAb114	REGN3479 + mAb114	2G4	4G7	ZMapp	KZ52
WT	1	1	1	1	1	1	1	1
P34S	0.6	0.4	0.4	0.5	0.7	0.6	0.6	0.5
P116H	0.6	0.6	>76.3[a]	0.8	0.7	0.7	0.9	0.6
G118E	0.5	0.4	>29.1[a]	0.5	0.9	0.7	0.7	0.5
G118R	0.6	0.5	>33.6[a]	0.6	0.9	0.7	0.8	0.6
T144M	1	1	>33.6[a]	1.1	1.1	1.1	1	0.9
G224D	0.6	0.6	1.3	0.8	0.7	0.7	0.7	0.7
E304A	0.7	0.7	0.5	0.6	0.3	0.2	0.4	0.4
T469I	0.8	0.7	0.6	0.7	0.9	0.7	0.6	0.7
Q508R	2.9	3.1	1.9	2.9	>88.3[a]	>77.3[a]	>73.5[a]	>69.5[a]
G528R	>361.5[a]	1.9	0.9	4	0.4	0.3	0.9	0.8
G557R	0.9	0.7	0.5	1	0.8	>74.5[a]	1.3	>77.1[a]
N563Y	>424.0[a]	0.9	0.4	3	0.5	>173.4[a]	>162.1[a]	>151.7[a]

[a]The change in mAb potency for this variant was calculated by dividing the maximal antibody concentration tested by the IC50 value for the WT pseudovirus. REGN3470, REGN3471, and 13C6 poorly neutralize lentivirus pseudovirus particles and could not be tested with escape variants. See also Figures S4 and S5.

KEY RESOURCES TABLE

REAGENT or RESOURCE	SOURCE	IDENTIFIER
Antibodies		
REGN3471	Regeneron	N/A
REGN3479	Regeneron	N/A
REGN3470	Regeneron	N/A
mAb114	Misasi et al.[26]	N/A
Alexa Fluor 488 secondary antibody	Invitrogen	A-11008
Polyclonal rabbit anti-VSV serum	Imanis Life Sciences	REA005-STAN
Anti-MARV VLP antibody	IBT Bioservices	04-0005
Mouse anti-human Fc mAb (REGN2567)	Regeneron	N/A
Bacterial and Virus Strains		
VSV-EBOV-GP	This manuscript	N/A
EBOV Mayinga	Rocky Mountain Laboratories, Dr. Heinz Feldmann	N/A
EBOV Mali	Rocky Mountain Laboratories, Dr. Heinz Feldmann	N/A
RESTV	Rocky Mountain Laboratories, Dr. Heinz Feldmann	N/A
BDBV	Rocky Mountain Laboratories, Dr. Heinz Feldmann	N/A
SUDV	Rocky Mountain Laboratories, Dr. Heinz Feldmann	N/A
MARV Musoke	Rocky Mountain Laboratories, Dr. Heinz Feldmann	N/A
MARV Angola	Rocky Mountain Laboratories, Dr. Heinz Feldmann	N/A
Chemicals, Peptides, and Recombinant Proteins		
Papain	Sigma	Cat# P3125
Iodoacetamide	Sigma	Cat# I6125
BioLock	IBA Lifesciences	Cat# 2-0205-250
Lauryl maltose neopentyl glycol	Anatrace	NG310
Ethanolamine	Cytiva	Cat# BR100050
Thermolysin L	Sigma	P1512-25mg
TRIzol Reagent	Life Technologies	Cat# 15596
Insect-XPRESS protein-free medium with L-glutamine	Lonza	12-730Q
Puromycin	Invivogen	ant-pr-5b
Critical Commercial Assays		
4D-Nucleofector X Kit L	Lonza	Cat# V4XC-2012
BrightGlo luciferase assay	Promega	E2610
Phosphate-buffered saline	Life Technologies	20012-043
Sucrose	Invitrogen	15503-022
Deposited Data		

REAGENT or RESOURCE	SOURCE	IDENTIFIER
Structure of EBOV GP (Mayinga) bound to three REGN 3471 fabs, two REGN 3470 fabs, and three REGN 3479 fabs	Protein Data Bank (rcsb.org)	PDB: 7TN9
Cryo-EM map of EBOV GP (Mayinga) bound to three REGN 3471 fabs, two REGN 3470 fabs, and three REGN 3479 fabs	Electron Microscopy Data Bank (https://www.ebi.ac.uk/emdb/)	EMD-26005
Experimental Models: Cell Lines		
HEK293T	ATCC	CRL-3216
Vero E6	ATCC	CCL-81
BHK-21	ATCC	CCL-10
Drosophlia S2	Thermo Fisher Scientific	Cat# R69007
Huh7	JCRB Cell Bank	JCRB0403
Recombinant DNA		
Empty vector: pMTpuro	Bunch et al.[40]	Addgene #17923
pMTpuro-EBOV Mayinga GP Ectodomain	West et al.[20]	N/A
pMTpuro-EBOV Mayinga GP DMLD	West et al.[20]	N/A
VSV-EBOV-GP	This manuscript	N/A
pVSV-N	Baum et al.[18]	GenBank: NC_038236
pVSV-P	Baum et al.[18]	GenBank: NC_038236
pVSV-G	Baum et al.[18]	GenBank: J02428.1
pVSV-L	Baum et al.[18]	GenBank: NC_038236
pT7	Baum et al.[18]	GenBank: NC_001604
pEBOV-GP-WT	This manuscript	GenBank: KJ660346
pEBOV-GP-P34S	This manuscript	N/A
pEBOV-GP-P116H	This manuscript	N/A
pEBOV-GP-G118E	This manuscript	N/A
pEBOV-GP-G118R	This manuscript	N/A
pEBOV-GP-T144M	This manuscript	N/A
pEBOV-GP-G224D	This manuscript	N/A
pEBOV-GP-E304A	This manuscript	N/A
pEBOV-GP-T469I	This manuscript	N/A
pEBOV-GP-Q508R	This manuscript	N/A
pEBOV-GP-G528R	This manuscript	N/A
pEBOV-GP-G557R	This manuscript	N/A
pEBOV-GP-N563Y	This manuscript	N/A
Software and Algorithms		
SWISS-MODEL	Waterhouse et al.[41]	https://swissmodel.expasy.org/
SerialEM	Mastronarde, 2005[42]	https://bio3d.colorado.edu/SerialEM/
cryoSPARC	Punjani et al.[19]	https://cryosparc.com/
Topaz particle picker	Bepler et al.[43]	https://github.com/tbepler/topaz
DeepEMhancer	Sanchez-Garcia et al.[44]	https://github.com/rsanchezgarc/deepEMhancer
Phenix, versions 1.19	Adams et al., 2010[45]	https://www.phenix-online.org

REAGENT or RESOURCE	SOURCE	IDENTIFIER
Coot	Emsley and Cowtan, 2004[46]	https://www2.mrc-lmb.cam.ac.uk/personal/pemsley/coot/
LigPlot+	Laskowski and Swindells[47]	https://www.ebi.ac.uk/thornton-srv/software/LigPlus/
UCSF Chimera	Pettersen et al.[48]	https://www.cgl.ucsf.edu/chimera/
UCSF ChimeraX	Pettersen et al.[49]	https://www.cgl.ucsf.edu/chimerax/
Inkscape	Inkscape Project[50]	https://inkscape.org/
Biacore T200 Evaluation software v3.1	Cytiva	CAT# 29148695
Microsoft Word	Microsoft	https://www.microsoft.com/en-us/microsoft-365/word
Microsoft Excel	Microsoft	https://www.microsoft.com/en-us/microsoft-365/excel
Molprobity	Williams et al., 2018[51]	http://molprobity.biochem.duke.edu/
OMIT maps	Terwilliger et al., 2008[52]	https://phenix-online.org/documentation/reference/composite_omit_map.html
Other		
StrepTrap 5mL HP	Cytiva	Cat# 28907547
MonoQ 5/50 GL	Cytiva	Cat# 17516601
Superdex 75 Increase 10/300 GL	Cytiva	Cat# 29148721
Superdex 200 Increase 10/300 GL	Cytiva	Cat# 28990944
Superose 6 Increase 10/300 GL	Cytiva	Cat# 29091596
Äkta Pure 25 Protein purification system	Cytiva	Cat# 29018224
Oryx Crystallization Robot	Douglas Instruments	https://www.douglas.co.uk
BIAcore T200 Instrument	Cytiva	Cat# 28975001
Sensor Chip CM5	Cytiva	Cat# 29104988
Titan Krios	Thermo Fisher Scientific	https://www.thermofisher.com/us/en/home.html
C-flat™ Holey thick carbon grids (CF-2/1-4C-T)	Electron Microscopy Sciences	https://www.emsdiasum.com/
PELCO easiGlow Glow Discharge Cleaning System	Ted Pella	https://www.tedpella.com/easiGlow_html/Glow-Discharge-Cleaning-System.aspx
Vitrobot Mark IV	Thermo Fisher Scientific	https://www.thermofisher.com/us/en/home/electron-microscopy/products/sample-preparation-equipment-em/vitrobot-system.html
SpectraMax i3 plate reader	Molecular Devices	Cat#i3
Immunospot Analyzer	Cellular Technology Limited	N/A
Nikon Ti2	Nikon	N/A
Victor X3 plate reader	PerkinElmer	N/A
Cytation 1 Multimode Plate Reader	Biotek	Cat# CYT1V
Amicon Ultra-15 Centrifugal Filter Unit 10kDa MWCO	EMD Millipore	Cat# UFC901008
Amicon Ultra-15 Centrifugal Filter Unit 100kDa MWCO	EMD Millipore	Cat# UFC910008